

Generalized mathematical model for adaptive cell survival after thermoradiotherapy: The impact of sublethal damage

Adriana M. De Mendoza^{1,2,+,*}, Soňa Michlíková^{2,3,+}, Steffen Lange^{2,4}, Paula S. Castro⁵,
Anni G. Muñoz¹, Lisa Eckhardt^{2,6,7,}, and Leoni A. Kunz-Schughart^{2,8,*}

¹Pontificia Universidad Javeriana, Physics Department, Bogotá, 110231, Colombia

²OncoRay—National Center for Radiation Research in Oncology, Faculty of Medicine and University Hospital Carl Gustav Carus, Technische Universität Dresden, Helmholtz-Zentrum Dresden — Rossendorf, 01307 Dresden, Germany

³Helmholtz-Zentrum Dresden-Rossendorf, Institute of Radiooncology - OncoRay, 01328 Dresden, Germany

⁴DataMedAssist Group, HTW Dresden—University of Applied Sciences, 01069 Dresden, Germany

⁵Universidad Distrital - Francisco José de Caldas, Bogotá, 111611, Colombia

⁶Core Unit for Molecular Tumor Diagnostics (CMTD), National Center for Tumor Diseases Dresden (NCT/UCC), Germany: German Cancer Research Center (DKFZ), 69120 Heidelberg, Germany

⁷German Cancer Research Center (DKFZ), Heidelberg, Germany, and German Cancer Consortium (DKTK), partner site Dresden, Germany

⁸National Center for Tumor Diseases (NCT), Partner Site Dresden, 69120 Heidelberg, Germany

* Author to whom correspondence should be addressed

+ These authors contributed equally to this work

ABSTRACT

The efficacy of radiotherapy (RT) can be significantly enhanced by combination with hyperthermia (HT), offering improved therapeutic outcomes at reduced radiation doses. Recent technological advancements have revitalized HT as a promising option for combinatorial RT. However, the underlying mechanisms, implications, and cause-effect relationships require further elucidation for precise integration into clinical practice. In this context, mathematical modeling provides the necessary predicting power for treatment planning. Moreover, based on physicochemical principles, such models help elucidate the behavior of biological systems under heat. Some cell cultures exhibit dose-dependent changes in therapy response and survival, prompting the development of a model incorporating cell recovery mechanisms. We extended Jung's model of cellular inactivation by heat based on the accumulation of sublethal damage to combinatorial radiotherapy in general and incorporated dose-dependent recovery rates. The resulting unified model (Umodel) is suited to describe (i) individual or sequential treatment/fraction outcomes, (ii) differences and changes in cellular response and recovery or adaptation to treatment, and (iii) the observed sensitivity to treatment order. We demonstrate excellent performance ($R^2 \gtrsim 0.95$) on various cell survival data from the literature and our own experimental series. Our observations suggest that the induction of sublethal damage in cells is pivotal, promoting cellular vulnerability for synergistic outcomes in combined therapeutic schemes.

Introduction

Radiotherapy (RT) continues to be the second most common medical intervention prescribed to more than half of the patients diagnosed with cancer^{1,2}. Even though RT is very effective in reducing the tumor mass, many times, the dose required to cure the patient cannot be applied due to high toxicity to the adjacent normal tissue. Therefore, an effective combination with radiosensitizing moieties is crucial for better (curative) therapeutic results at lower radiation doses. Heat is one of the most potent radiosensitizers, achieving thermal enhancement ratios (TER) as high as 8.0 *in vivo* studies³⁻⁶. The combination of ionizing radiation with heat, also known as thermoradiotherapy (TRT), has been shown to attain the highest TER when applied simultaneously^{3,4,7,8}. However, the clinical implementation of simultaneous TRT treatments is not yet a reality due to technological and logistical limitations^{3,9-11}. Nevertheless, sequential TRT with varying treatment orders and gaps between the individual modalities combined with or without chemotherapy is an active field in clinical research, with 45 clinical trials to this date reported active or completed^{12,13}. Furthermore, the growing number of recent topic-related publications evidences the revival of hyperthermia cancer research and treatment, mainly motivated by state-of-the-art advances in a localized, spatially and temporally controlled heat application¹⁴⁻²⁰.

Tumor response to treatment and prediction of patient survival are both based on cell survival models, which are translated by mathematical approaches or simulations into tumor control probabilities (TCPs)²¹⁻²³. Hence, accuracy in survival models is a critical component of the clinical workflow. On one hand, underestimation of cell killing can lead to overtreatment with unnecessarily high radiation doses, resulting in unwanted side effects and other related problems. On the other hand, if the model overestimates cell killing, the treatment will be planned with radiation doses insufficient to control the malignancy, thus resulting in tumor relapse but still accompanied by side effects. Different mathematical models have been designed to predict the effect of radiation and hyperthermia therapies, and empirical approaches exist also for their combination. However, a model capable of describing cell survival from shared general principles upon any of the two treatments individually or concomitantly applied is yet to be available. For ionizing radiation, the LQ model offers one of the best and most robust approaches to predicting the survival fraction in RT treatments²⁴. Nonetheless, due to its mechanistic nature based on the probability of radiation-induced DNA breakage, the LQ model is not suited to describe the effects of hyperthermia. Moreover, the LQ model has limitations, particularly at low-survival or high-dose regimes, where the cell kill is overestimated, i.e., at the tail of the logarithmic survival curve, which is typically straight²⁵. Some alternative models deal with this issue by including empirical terms^{26,27}. There are also several mathematical models for HT-induced cell killing, with a very poor consensus²⁸⁻³². When it comes to TRT, mathematical modeling contributes to prediction and a better understanding of the synergistic effects of the combined therapy and aids in the identification of the most suitable administration schedule. A synergistic component describing the HT-induced radiosensitization has to be included in addition to the cumulative cell killing by the two individual therapies. Our previous publication summarized the available models predicting cell survival upon thermoradiotherapy³³. At this point, we want to emphasize that these models - although providing good empirical approximations ($R^2 \gtrsim 0.95$) - can still neither describe the effect of both mono-treatments nor the impact of the sequential application (HT → RT or viceversa) and the time-lapse (gap) between the two treatment modalities. More mechanistic approaches are offered by the *Repair-Misrepair model*³⁴, the *Local Effect Model (LEM)*³⁵ and the *Giant Loop Binary Lesion model*³⁶, but these are suited explicitly for RT.

An appropriate model to encompass the effects of heat and irradiation in mono- and combination treatments must allow the accumulation of sublethal damage (SLD). To our knowledge, two HT response models incorporate this feature^{29,31}. We previously developed a model for simultaneous TRT based on thermodynamic principles, where radiosensitization is described as an accumulation of HT-induced SLD³³. Here, we propose Jung's model as a suitable basis. It stipulates that cells lose their proliferative capacity due to damage accumulation in discrete stages without reliance on a particular biological mechanism. This assumption provides an advantage to describe the harm induced by any therapy (i.e., ionizing radiation or heat). Jung's model very well describes cell clonogenic survival under HT and RT mono-treatments. However, it does not contain components describing changes in SLD restoration rates. Thus, it cannot reflect the effects of HT on the repair of RT-induced DNA damage, a fundamental process in HT-induced radiosensitization. Restoration parameters are also required for modeling the outcome of combinatorial therapies that are applied consecutively with a gap. Moreover, due to this limitation, Jung's model fails to reproduce clonogenic curves, which can be affected by changes in cell population recovery with increasing thermal or radiation dose, e.g., changes in the kinetics of DNA-repair, protein refolding, metabolic adaptations, the existence of resistant subpopulations, among others. These effects might be expressed as straightening or flattening of the clonogenic cell survival curves. Such behavior can be a possible cause of cell-killing overestimation that is usually not accounted for in the mathematical survival models.

Here, we present a modification of Jung's model by incorporating a dose-dependent rate of SLD recovery. The recovery rate is modeled as an effective enzymatic reaction, accounting for all possible restoration mechanisms of accumulated non-lethal damage at the cellular or the population level. To describe the radiosensitizing effect of HT, we further incorporate the possibility of reducing the repair rates for the RT-induced damage when applied together with HT. These modifications improve the accuracy in predicting dose-response relationships and potentially enable recovery during the gap in sequential treatment applications. We tested the performance of our "unified" model (Umodel) on various cell survival data from literature and our experimental data in a panel of human head and neck squamous cell carcinoma (HNSCC) cell lines, where HT and RT were applied individually and in combination. The goodness-of-fit was compared to the standard LQ and Jung's models, yielding comparable or superior results. Our findings support using the Umodel for accurate predictions of cell survival upon sequential TRT in treatment planning. The report ends by discussing the advantages and limitations of the newly developed Umodel, giving an outlook, and suggesting possible future uses and improvements.

Methods

Development of the “Umodel”

Monotreatment

Original Jung’s model

Jung’s model considers an infinite number of stages, also called compartments, of SLD accumulation. At the n -th stage, there is a fraction of surviving cells enduring n non-lethal lesions. The probability that the cell is in the n -th compartment is given by the solution of the detailed balance equation

$$\frac{dP_n(t)}{dt} = -rP_n(t) - ncP_n(t) + rP_{n-1}(t), \quad (1)$$

which is a time-continuous Markov chain. It describes the time evolution of the probability at the n -th compartment in a way that cells can advance in a sequence of SLD with a rate r , or escape to death with a rate nc , proportional to the stage of non-lethal damage accumulation (see Fig.1). Here, r is defined as the rate of SLD accumulation, and c is the rate of damage fixation, which refers to processes that prevent further damage repair in a non-reversible manner. Thus, the state of the cell population can be described by a probability vector $\vec{P}(t) = (P_0(t), P_1(t), P_2(t), \dots, P_n(t), \dots)^T$, whose n -th element is the probability that the cell is in n -th compartment at time t . Jung’s original model was proposed to describe the effect of heat on *Chinese hamster ovary* (CHO) cells *in vitro*, reproducing very well the HT outcome²⁹. There, the advance rate r between consecutive compartments in the chain of non-lethal damage is constant.

Equation 1 is solved under the following boundary conditions:

1. At the first compartment ($n = 0$) cells are not yet damaged by the treatment. Therefore, it is only possible to move forward at the onset of the treatment $\frac{dP_0(t)}{dt} = -r_0P_0(t)$.
2. At $t = 0$, just before treatment starts, $P_0(0) = 1$ and $P_n(0) = 0$ (for $n \geq 1$). This means that the initial condition can be written as the state vector $\vec{P}(t = 0) = (1, 0, 0, 0, \dots, 0)^T$.
3. Cell killing requires damage, hence the cell undergoes through at least one stage of damage before dying.

To solve Eq. 1, the evolution of the state vector can be written as $\frac{d\vec{P}(t)}{dt} = \hat{A}\vec{P}(t)$, where the elements of the transition matrix \hat{A}_{ij} define the influx rate from $n = j$ to $n = i$, and the diagonal elements are the net flux at each stage. The survival probability is given by the probability of being in any of the non-lethal damage compartments:

$$S(t) = \sum_{n=0}^{\infty} P_n(t). \quad (2)$$

In Jung’s original model, the applied thermal dose is proportional to the treatment time for a fixed heat intensity (determined by the temperature) $D = \dot{D}(T)t$. When cellular damage is inflicted, the biological response is triggered and may take seconds to days to complete^{37,38}. Hence, ongoing damage, recovery, or death may not occur during treatment, but cells are poised to suffer damage, die (lose proliferative capacity), or get repaired in response to the applied dose. Thus, time refers to treatment duration, while the rates of damage advancement and fixation depend on the dose rate \dot{D} . In the case of treatment with ionizing radiation, the dose rate is usually predetermined in experiments by the power of the irradiator in such a way that the desired total dose is administered by adjusting the exposure time. In HT treatments with conventional heat sources, the dose rate is the pace of heat deposition and is related to temperature. Therefore, the treatment temperature is set in HT experiments, and total thermal dose is determined by the exposure time.

Regression rate in Jung’s model

Jung’s model does not include the possibility of regressing in the chain of SLD. We incorporate this feature to describe adaptation to treatment and tissue recovery during gaps between treatment applications. Since recovery can be stimulated or

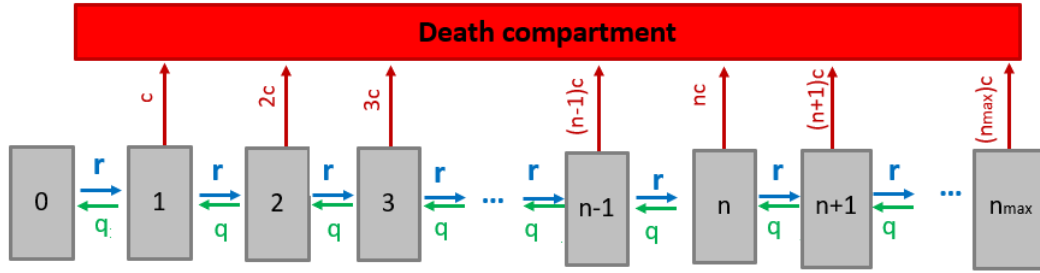


Figure 1. Compartment model of cell killing by HT. Original Jung's model without regression rates q ²⁹. Our proposed modification called Umodel includes regression rates q (green arrows).

dampened in response to the inflicted damage, we consider two possibilities: regression rate q dependent either on the stage of damage n or on the treatment time t . When an n -dependent regression rate q_n is included in Jung's model, the net advance rate $r_n = r - q_n$ changes with the level of SLD. The general solution of $P_n(t)$ is presented in Section I of the supplementary information (SI-Eq. 2), and the survival probability is given by $S(t) = \sum_{n=0}^{n_{max}} P_n(t)$, where we have assumed that a finite number n_{max} of SLD stages are populated. We tried different stage-dependent functions for q_n (described in the SI- Eqs. 4-6), but the results yielded no improvement over the original Jung's model.

After ruling out a stage-dependent regression, we examined a dose-dependent regression function, i.e. treatment time t for a fixed \dot{D} . The inclusion of a time-dependent function $q(t)$ makes the transition matrix $\hat{A} \rightarrow \hat{A}_t$ time-dependent too. In this particular case, the detailed balance equation reads

$$\frac{dP_n(t)}{dt} = -r(t)P_n(t) - ncP_n(t) + r(t)P_{n-1}(t), \quad (3)$$

$$\text{where } r(t) = r - q(t). \quad (4)$$

The solution is approximated at first order in the Magnus expansion as

$$\vec{P}(t) = e^{\hat{A}_t} \vec{P}(t=0), \quad (5)$$

with integrated transition matrix $\hat{A}_t = \int_0^t dt' \hat{A}(t')$ is equal to

$$\hat{A}_t = \begin{pmatrix} -\int_0^t dt' r(t') & 0 & \dots & 0 \\ \int_0^t dt' r(t') & -\int_0^t dt' (r(t') + c) & \ddots & \vdots \\ 0 & \int_0^t dt' r(t') & \ddots & \\ \vdots & \ddots & \ddots & 0 \\ 0 & \dots & 0 & -\int_0^t dt' (r(t') + (n_{max} - 2)c) & 0 \\ & & & \int_0^t dt' r(t') & -\int_0^t dt' (r(t') + (n_{max} - 1)c) \end{pmatrix}. \quad (6)$$

Since it is not possible to calculate all the contributions from the infinite series, we assess the error as the contribution of the next order, assuming that each next order contributes less and less for a repair function that is saturating to a constant value. Moreover, if the parameter k is small compared with treatment time, the time-dependent regression rate saturates fast to a constant value, and the error does not increase with treatment time. Therefore, we calculated the error of $\vec{P}(t)$ as the difference between the probabilities at first and second order, which shows a small error when the parameters are almost constant for the most of the treatment time. As an example, using the Umodel's parameters obtained for UT-SCC-14 cells under 44.5°C HT, the

error values ranged below 10^{-4} at $t = 1$ min, and below 10^{-46} at $t = 60$ min (more details shown in SI Sec. 2).

As radiation- and heat-induced damage is detected and restored by enzymatic mechanisms, we propose to model the regression process (in time) by means of an “effective” enzymatic reaction representing the average kinetics of the restored molecules in the cell population. Detailed mathematical models have been proposed to describe some of the reactions taking part in DNA-repair and protein refolding, introducing and numerically solving large sets of coupled differential/integral equations^{25,39–45}. These frameworks lead to the required regression rates but need many adjustable parameters, making those approaches unsuitable for practical survival models. Therefore, for the sake of simplicity, we introduce a source (damage) term into the Michaelis-Menten (MM) model, which consists of four differential equations describing the following enzymatic chemical reaction:



Here $[E]$, $[S]$, $[P]$, denote the concentrations of the enzyme, the substrate (damaged molecule), and the product (restored molecule), respectively; and $[E \cdot S]$ is the concentration of enzyme-substrate intermediate complex. In this equation, the enzyme E is associated to a substrate molecule S . This step occurs with rate k_f but can also be reversed with rate k_r . After the interaction, the enzyme dissociates unchanged, and the substrate turns into a product molecule P . This part of the process occurs with a rate of catalysis k_{cat} ⁴⁶. After including the source of damage r into the substrate and product equations, the time-evolution of the concentrations is given by:

$$\begin{aligned} \frac{d[E]}{dt} &= -k_f[E][S] + (k_r + k_{cat})[E \cdot S] \\ \frac{d[S]}{dt} &= -k_f[E][S] + k_r[E \cdot S] + r \\ \frac{d[E \cdot S]}{dt} &= k_f[E][S] - (k_r + k_{cat})[E \cdot S] \\ \frac{d[P]}{dt} &= k_{cat}[E \cdot S] - r[P]. \end{aligned} \quad (8)$$

Since the source term r in the substrate kinetics is the rate of SLD production, it connects the enzymatic process with Jungs’ model. Under the quasi-steady state approximation, the enzyme-substrate complex is assumed to be constant ($\frac{d[E \cdot S]}{dt} = 0$). Accordingly, after upregulation, the total enzyme concentration is constant ($\frac{d[E]}{dt} = 0$ and equal to the initial value $[E] + [E \cdot S] = [E]_0$). The net rate of molecular mending $\frac{d[P]}{dt}$ is obtained by subtracting the damage rate from to the damage regression rate $\frac{d[P]}{dt} = q(t) - r[P]$, meaning that the regression rate can be modeled as:

$$q(t) = k_{cat}[E \cdot S] = \frac{q_{max}[S]}{k' + [S]}, \quad (9)$$

where $q_{max} = k_{cat}[E]_0$, and $k' = \frac{k_r + k_{cat}}{k_f}$. The solution of Eq. 8 for the concentration of impaired molecules (substrate) reads

$$[S] = \frac{k'}{q_{max} - r} \left[r + q_{max} W_0 \left(\frac{-e^y}{k q_{max}} \right) \right] \quad (10)$$

W_0 is the principal branch of the Lambert function, with $y = \frac{(q_{max} - r)^2 t - k r}{k q_{max}}$. Since $[S]$ is a monotonically increasing function of time, we keep it to first order in the Taylor expansion $[S] \sim [S]_0 + r t$ to simplify the model. This approximation is valid in the regime of slow advance rates. Assuming also $[S]_0 = 0$ at the beginning of the treatment, Eq. 9 gets

$$q(t) = \frac{d[P]}{dt} = \frac{q_{max} t}{k + t}, \quad (11)$$

with $k = k'/r$ being the average time to achieve the half of the maximum cellular capacity of mending impaired molecules. With this approach, we get a sigmoid rise of the repaired molecules in time, consistent with the functional forms obtained in references^{25,40}, but with just two adjustable parameters. By inserting Eq. 11 into Eq. 4, the survival probability reads:

$$S(t) = \exp \left\{ \frac{\int_0^t r(t') dt'}{ct} [1 - ct - e^{-ct}] \right\}, \quad (12)$$

with $\int_0^t r(t') dt' = rt - q_{max} \left[t + k \ln \left(\frac{k}{k+t} \right) \right]$. It is worth mentioning that treatment time can be exchanged by the total dose ($t \rightarrow D$) in Eq. 12, given that the dose rate is constant throughout the treatment. This variable substitution only changes the units of the adjustable parameters r, c, q_{max} and k .

Combined treatment

There are two very interesting and not fully elucidated aspects concerning the combination of RT and HT treatments. Firstly, the outcome of the combinatorial therapy is not additive but rather synergistic. Secondly, the order in which the therapies are applied affects the therapeutic benefit, meaning that the therapies do not commute^{4,47-50}. Furthermore, these two characteristics manifest within a limited time lapse between the two treatments^{4,50}. The original Jung's model can still describe this non-commutativity (asymmetry), as we show in detail below. However, the radiosensitizing effect of heat needs to be incorporated, including the impact of the gap between consecutive applications. The latter requires the regression function obtained in Eq. 11 to describe the cellular recovery taking place during this time. These effects are mathematically formulated from the general concepts of SLD accumulation and restoration. Further assessing any specific underlying biological mechanisms is out of the scope of this work.

Asymmetry and synergy

The outcome of two sequential treatments is obtained in our model by calculating the vector state $\vec{P}(t_1, t_2)$ after the administration of the two therapies labeled 1 and 2. This can be done by applying sequentially the transformation matrices \hat{A}_{t_1} and \hat{A}_{t_2}

$$\vec{P}(t_1, t_2) = e^{\hat{A}_{t_2}} e^{\hat{A}_{t_1}} \vec{P}(0). \quad (13)$$

Note that the exponentials in Eq. 13 do not commute $\exp(\hat{A}_{t_2}) \exp(\hat{A}_{t_1}) \neq \exp(\hat{A}_{t_1}) \exp(\hat{A}_{t_2})$, naturally incorporating into the model the effect of the sequence in the therapeutic outcome. Even if \hat{A}_{t_2} and \hat{A}_{t_1} do not affect each other, and omitting for the moment the recovery taking place between treatments, the Baker-Campbell-Hausdorff (BCH) formula allows to identify enhancement terms arising from the mathematical fact that the operators representing the individual therapies do not commute. Keeping up just to second order, the cellular state can be written as

$$\vec{P}(t_1, t_2) \approx \left(e^{\hat{A}_{t_2} + \hat{A}_{t_1} + \frac{1}{2} [\hat{A}_{t_2}, \hat{A}_{t_1}]} \right) \vec{P}(0), \quad (14)$$

with $[\hat{A}_{t_2}, \hat{A}_{t_1}] \equiv (\hat{A}_{t_2} \cdot \hat{A}_{t_1} - \hat{A}_{t_1} \cdot \hat{A}_{t_2}) \neq 0$. Equation 14 shows that asymmetry and enhancement are closely related. An enhancement term in the exponential arises, which depends on the sequence of the treatments. The exponentials in Eq. (13) only commute when the respective transition matrices commute, which does not happen for different treatments. In that case, the treatments become independent without neither enhancement nor asymmetry. According to Eq. (14), the additive effect is given by $(\hat{A}_{t_2} + \hat{A}_{t_1})$ in the exponent, and the enhancement term arises from the commutator $[\hat{A}_{t_2}, \hat{A}_{t_1}]$. Since $[\hat{A}_{t_2}, \hat{A}_{t_1}] = -[\hat{A}_{t_1}, \hat{A}_{t_2}]$, it should be noted that the opposite sequence would lead to a different therapeutic outcome, as detailed below. Calculating the commutator, we get a matrix with all the elements being zeros except subdiagonal elements (X)

$$[\hat{A}_{t_2}, \hat{A}_{t_1}] = \begin{pmatrix} 0 & 0 & \dots & 0 \\ X & 0 & \dots & 0 \\ 0 & X & \dots & 0 \\ \vdots & \ddots & \dots & 0 \\ 0 & \dots & X & 0 & 0 \\ 0 & \dots & 0 & X & 0 \end{pmatrix}. \quad (15)$$

with non-null terms:

$$X = \left[\int_0^{t_1} r_1(t') dt' \right] [c_2 t_2] - \left[\int_0^{t_2} r_2(t') dt' \right] [c_1 t_1], \quad (16)$$

From Eq. 16 it can be seen that the commutator, and therefore the synergy between the treatments, increases when the first treatment induces more sublethal damage than damage fixation, and the second treatment does the opposite. Consequently, the more lethal therapy should be applied second to enhance the synergy in the combined scheme. It is important to mention that this implication is valid only if the first treatment does not induce tolerance to the second one, as may be the case for the combining two HT therapies in the step-up protocol⁵¹.

In order to better understand why the treatment outcome depends on the sequence, let's assume that the cells are sensitized by the first treatment to die more easily during the second one. Hence, if the damage inflicted during the first treatment is not mended, the cell encounters damage fixation and cell death with the second treatment. The cells suffering SLD on the first treatment will be vulnerable to die by damage fixation either upon the first treatment or the second one, having two channels to shift to the death compartment. Therefore, the sequence that maximizes SLD on the first treatment becomes more effective because of the larger amount of cells previously sensitized to die. For RT combined with HT, the less lethal treatment is typically hyperthermia, explaining why the thermal enhancement ratios reported for HT→RT are usually bigger than the other way around^{4,49}.

Note that in principle also time lapses (gaps) between treatments can be incorporated through a “gap” operator \hat{A}_g between \hat{A}_{t_1} and \hat{A}_{t_2} , which describes recovery taking place between treatments/applications (see SI Section 3 for details). Combinatorial treatments with and without gaps can also be formulated uniformly in chronological time instead of treatment dose. However, calibrating the corresponding model parameters would require additional analytical endpoints of cell recovery, damage, and death after treatment, which can be reliably monitored over short and intermediate times. The corresponding systematical data have to be acquired in the future by specifically designed experiments.

Treatments interaction: miss-repair hypothesis

Besides the synergy due to non-commutativity, it is also possible that one treatment affects the rates r or c of the other. One of the most plausible mechanisms to explain, at least partially, the thermal enhancement of ionizing radiation is the impairment of the DNA-repair mechanisms that restore the radiation-induced damage. McMahon and Prise proposed a mathematical model to predict the radiosensitivities of cells based on the failure probability of the repair mechanisms⁵². However, its inclusion into the Umodel would critically increase the number of adjustable parameters, not only increasing the complexity of the model but necessitating the use of large data sets (with many experimental points on the dose-response curves) that are usually not available. Therefore, and for the sake of simplicity, we included repair impairment in our model by means of a reduced repair rate of the DNA damage induced by RT. This repair rate is reduced by a quantity $q_{red}(T_{HT}, t_{HT})$, which depends on the hyperthermia treatment and leads to an augmented SLD rate $r_{RTnew} = r_{RTold} + q_{red}(t_{HT}, T_{HT})$.

$$ER = \frac{r_{RTnew}}{r_{RTold}} = 1 + \frac{q_{red}(t_{HT}, T_{HT})}{r_{RTold}}. \quad (17)$$

The functional form of the enhancement ratio ER here depends on the effect of HT on DNA-repair, which from thermodynamic considerations³³; is (i) linear with HT-treatment time and (ii) exponential with HT-treatment temperature. With these considerations accounted for, ER reads

$$ER = 1 + t e^{b(T-T_g)}. \quad (18)$$

Furthermore, we speculate that the damage fixation rates of RT (c) may also be affected by HT. For instance, the complete break of the DNA double helix after RT often requires the repair endonucleases. Hence, the thermal denaturation of endonucleases may reduce the rate of damage fixation and will, in turn, lead to reduced amounts of DSBs^{53,54}.

The operators' formalism used in the Umodel to describe of the sequential treatment provides a calculation tool that allows a step-by-step description of the treatments' effects on cell populations, at the cost of only two additional adjustable parameters. Our model goes beyond the mere adjustment of data, predicting the effect of the applied doses (radiation or heat) at different instances of the combined treatment.

Multiparametric optimizations

We use non-linear least-square minimization provided by the python package *lmfit*⁵⁵ to fit the required parameters of each model, i.e., the radiosensitivities (α, β) of the LQ-model, the advance and damage fixation rates (r and c) of Jung's model, and the parameters (r, c, q_{max} and k) of the Umodel (see Eqs. 12 and 13). All values are adjusted using the Levenberg-Marquardt algorithm^{56,57} to fit the corresponding biological effect ($-\ln(S)$), experimentally obtained from the survival assays. The parameters are determined by minimizing the residuum ϵ of the biological effect

$$\epsilon = \sum_i [\ln S_i - \ln f_S(x_i, \{\gamma\})]^2. \quad (19)$$

Here i is a label for each survival probability S_i in the experimental data set, $\{\gamma\}$ is the set of adjustable parameters, and $f_S(x_i, \{\gamma\})$ is the corresponding prediction of the survival probability from the applied model. We set reasonable boundaries for the parameters, i.e., typically $r[\text{min}^{-1}] \in [0, 50]$, $c[\text{min}^{-1}] \in [0, 1]$, $q_{max}[\text{min}^{-1}] \in (0, 50]$, $k[\text{min}] \in (0, 1]$, $\alpha[\text{Gy}^{-1}] \in [0, 1]$ and $\beta[\text{Gy}^{-2}] \in [0, 1]$. Note that, while any fit for r and c in Jung's model is in principle also valid for the Umodel with $q_{max} = 0$, we explicitly restrict the minimization to different parameters' values ($q_{max}, k > 0$).

It is important to note that the existence of several local minima for the error function hinders the search for a global solution. This implies that different values of adjustable parameters may produce similar values of $R^2 \sim 1$. This disadvantage is called "lack of identifiability", a major problem in mathematical models of biological systems^{58–60}. It is worth mentioning that the lack of identifiability refers to the existence of correlations among the parameters and does not necessarily imply *overfitting*, i.e., redundant parameters in the model. For instance, the parameters α and β of the LQ model are very identifiable, while Jung's model lacks identifiability, both models having two adjustable parameters. In our model, the lack of identifiability is inherited from Jung's original model. To help overcome this problem, we restrict the solution space to parameters that satisfy the thermodynamic prediction described in³³. This condition improves the identifiability of the parameters in HT but does not fully solve it. The thermodynamic condition states that the SLD rate should grow exponentially with treatment temperature, as described in section . Hence, for the Umodel in HT, r is also restricted to depend exponentially on temperature. To implement this restriction, the parameters at all temperatures T are optimized simultaneously for each cell line, and the deviation of the function $r(T)$ from a linear fit $\log[r(T)] = b(T - T_g)$, is added to the residuum. Moreover, we presumed that the maximum repair rate q_{max} would follow the trend of the inflicted damage. Hence, to reduce the ambiguity of the fitted parameters, we similarly imposed the exponential condition on q_{max} , for which the model reproduces the experimental data equally well. In the combined sequential treatment, heat-induced denaturation of repair proteins is implemented by changing the original rates r and c of the radiation treatment. Accordingly, these two parameters are readjusted, forcing the thermodynamic conditions on the new r , which should depend exponentially on temperature and linearly on HT treatment time³³. In all the cases, the resulting goodness-of-fit is reported by the coefficient of determination R^2 with respect to the survival fraction. Like other multiparametric optimization methods, the Levenberg-Marquardt algorithm is an iterative procedure that depends on the initial estimate of the parameter set $\{\gamma\}_0$ and only converges to the global minimum if the initial estimate is already close to the solution.

Inclusion criteria for experimental data sets from the literature

Cell survival curves as a function of the applied dose were included only if they presented at least five experimental data points per curve. For RT alone, we exclusively considered survival curves displaying dose-dependent flattening. In these data sets, the dose needed to be given in Gy and the irradiation power reported in the original articles. For HT alone, the dose had to be expressed as treatment time for at least three different temperatures. For sequential TRT, the survival curves of the combined treatment should be functions of radiation dose for at least two HT treatments with different times and temperatures. For the Umodel to be used on those data sets, it was additionally required that dose-response curves for the individually applied RT and HT treatments, as well as the treatment order and gap between them, were reported. Experimental points and error bars (when reported) from each data set were extracted using *WebPlotDigitizer*^{6R}. The names of the cell models follow the Cellosaurus nomenclature.

Experimental methods

Cell culture

Eight human HPV-negative HNSCC cell lines were used in this study: SAS and HSC4 (HSRRB/JCRB, Osaka, Japan), UT-SCC-5, UT-SCC-14, and UT-SCC-60A (University of Turku, Finland), Cal33 (DSMZ, Germany), XF354 (DKFZ, Germany),

and a subline of the FaDu-ATCC HTB-43 model (Dresden, Germany)⁶¹. The genetic profile was verified via microsatellite analyses at the Institute of Legal Medicine (TU Dresden, Germany) before use. All cell lines were routinely tested free of mycoplasmas using a PCR Mycoplasma Kit (AppliChem, Darmstadt, Germany), as described previously⁶². The cell cultures were grown from validated frozen stocks for >2 to 620 passages (<120 cumulative population doublings) and cultured in standard Dulbecco's Modified Eagle Medium (DMEM) with L-glutamine, D-glucose (1 g/L) and 25 mM HEPES supplemented with 10% heat-inactivated fetal calf serum (FCS) and 1% penicillin/streptomycin (10,000 U/mL/ 10 mg/mL). Cells were kept in a humidified air atmosphere with 8% CO₂ at 37 °C. All culture media, supplements, solutions, and buffers were purchased from PAN- Biotech (Aidenbach, Germany).

Hyperthermia and irradiation

Exponentially growing cultures were enzymatically dissociated using 0.05% trypsin/0.02% EDTA in phosphate-buffered saline (PBS) to obtain single-cell suspensions. A CASY® TTC analyzer (Roche Innovatis, Reutlingen, Germany) was used to monitor cell culture quality and assess cell numbers and volumes in single-cell suspensions for further processing. Cells were then diluted appropriately and seeded in 6-well plates using 1 ml of medium in cell line- and treatment temperature-dependent concentrations. Cells were incubated at 37 °C for 24 h (less than one culture doubling) to allow adherence. All hyperthermia treatments were performed using a pre-heated temperature-controlled PST-60HL-4 Plate Thermo-Shaker (BioSan, Latvia). The 6-well plates were placed into the pre-heated shaker for defined treatment times at temperatures comprising the entire heating period - starting from the placement of the plates in the device to their removal. Control plates were incubated in parallel at 37 °C in the standard incubator. Cells were irradiated at room temperature with single doses of 0 – 6 Gy (200 kV X-rays; 0.5-mm Cu filter, approx. 1.32 Gy/min). In combination treatments, hyperthermia was immediately followed by irradiation (within 1 minute after the hyperthermia treatment). After completion of any type of treatment, 1 ml of DMEM medium was added to each well. The cultures were incubated for 7 – 14 days to allow colony formation, according to ≥5 cell line specific doublings under standard conditions. The colonies were washed with PBS, fixed for 10 min with 80% ethanol, and stained with Coomassie blue solution. Colonies with ≥50 cells were manually counted at low magnification. Plating efficiency and survival fraction were calculated.

Results and Discussion

In this work, we primarily developed a mathematical model to describe best the clonogenic survival upon radiation, hyperthermia, and their combination. The following sub-chapters present the results of multiparametric optimizations, showing at least one set of parameters yielding good performance in every case. The goodness-of-fit of the proposed model was compared with standard LQ- and Jung's model of cellular deactivation by heat. Although Jung's model was initially designed to describe cell survival after heat exposure, we here show for the first time that it is also suitable to reproduce clonogenic survival upon irradiation. As Jung's model is based on the accumulation of damage regardless of the energy type and specific underlying biological mechanism, it appears as a versatile candidate for modeling both mono- and combined therapy outcomes. However, Jung's basic model does not comprise a component of cellular recovery, which is essential to (i) describe the effect of heat on proteins of the DNA damage repair machinery, (ii) reflect the survival of cell populations displaying changes in cellular recovery with increasing dose, and (iii) predict the effect of a putative time gap in sequentially combined treatment, where recovery may take place after damage induction by the first therapy before the second one is applied. Therefore, we propose a modified Jung's model (termed Umodel) that mathematically incorporates a regression rate (see Methods section). We applied the LQ-, Jung's and the Umodel to dose-response survival curves recorded in our laboratory for several HNSCC cell lines exposed to RT and HT monotreatments or their combination and to additional data reported in the literature. Table 1 summarizes all experimental datasets used for the model fitting; the inclusion criteria have already been detailed in previous section).

Table 1. Description of data sets with their sources and treatments.

Monotreatment data: RT or HT individually applied						
Source	Cell line	Entity (cell type)	Treatment	HT temperatures [°C]	RT	Displays flattening HT
Experiment	Cal33	human HNSCC	HT,RT	42.5, 44.5, 46.5	no	no
	HSC4	human HNSCC	HT,RT	42.5, 44.5, 46.5	no	no
	SAS	human HNSCC	HT,RT	42.5, 44.5, 46.5	no	no
	FaDu	human HNSCC	HT,RT	42.5, 44.5, 46.5	no	no
	XF354	human HNSCC	HT,RT	42.5, 44.5, 46.5	no	no
	UT-SCCC-5	human HNSCC	HT,RT	42.5, 44.5, 46.5	no	no
	UT-SCCC-8	human HNSCC	RT	-	no	no
	UT-SCCC-14	human HNSCC	HT,RT	42.5, 44.5, 46.5	no	at 44.5°C
	UT-SCCC-45	human HNSCC	HT,RT	42.5, 44.5, 46.5	no	no
	UT-SCCC-60A	human HNSCC	HT,RT	42.5, 44.5, 46.5	no	no
29	CHO	chinese hamster ovary	HT	40, 41, 41.5, 42, 42.5, 43.5, 44, 44.5	-	no
63	Hela	human cervical carcinoma	HT	41, 42, 43, 44, 45	-	at 41, 42, 43 °C
64	CFU-MG	murine bone marrow	HT	41.8, 42, 42.3, 42.5, 43, 44	-	at 42, 42.3 °C
65	CCD-18Lu	granulocyte-macrophage progenitor normal human lung fibroblasts	HT	41, 43, 45	-	at 41, 43, 45 °C
65	WiDr	human colon carcinoma	HT	41, 43, 45	-	at 41, 43 °C
65	A549	human lung carcinoma	HT	41, 43, 45	-	at 41, 43, 45 °C
65	U87MG	human glioblastoma-astrocytoma	HT	41, 43, 48	-	at 43 °C
32	CHO	Chinese hamster ovary	HT	41.5, 42, 42.5, 43, 43.5, 44, 44.5	-	at 41.5, 42, 42.5 °C
47	CHO	Chinese hamster ovary	HT	42.2, 42.3, 42.4, 42.5	-	all
66	HepG2	human hepatoblastoma	RT (12C)	-	yes	-
66	HepG2	human hepatoblastoma	RT (16O)	-	yes	-
66	HUH7	hepatocellular carcinoma	RT (12C)	-	yes	-
66	PLC	hepatocellular carcinoma	RT (12C)	-	yes	-
67	SW1353	human chondrosarcoma	RT (12C)	-	yes	-
67	HDF	normal human dermal fibroblasts	RT (12C)	-	yes	-
68	CHO-xrs-5	X-ray hypersensitive mutant of CHO	RT (12C)	-	yes	-

Combined treatment data: HT and RT sequentially applied			
Source	Cell line	Treatment	HT temperatures [°C]
Own data	SAS	HT+RT	40.5, 42.5, 44.5
	FaDu	HT+RT	40.5, 42.5, 44.5
26	HCT-116	HT+RT	45, 46, 47
69	CHO	HT+RT	42.5, 43

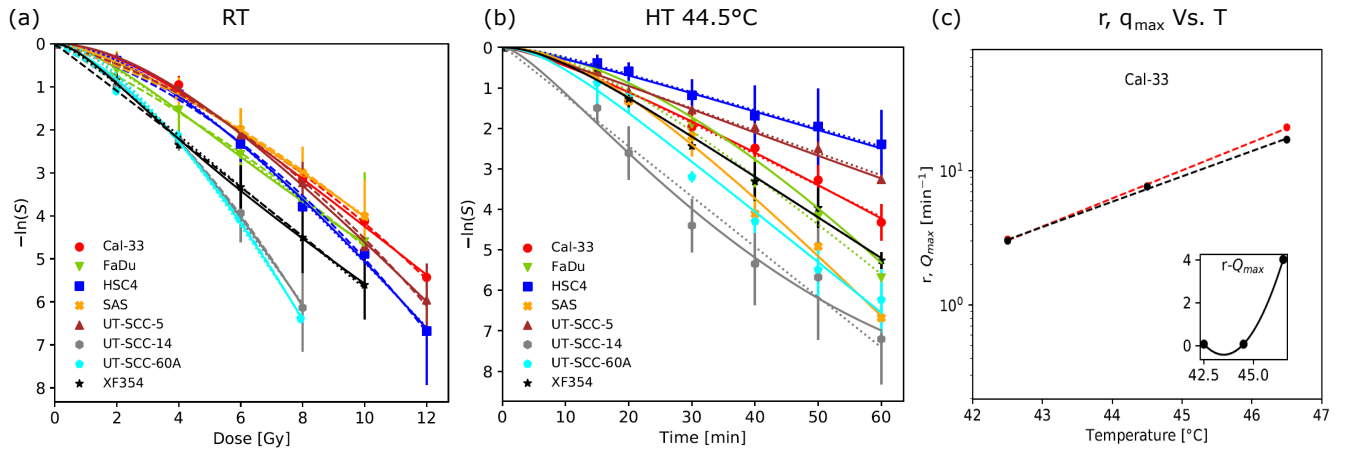


Figure 2. Comparison of LQ and Umodel in RT and HT clonogenic survival experiments. Symbols represent cell survival fractions ($-\ln(S)$) obtained from clonogenic assays using eight human HNSCC cell lines exposed to (a) 0-12 Gy RT⁶² and (b) HT at 44.5°C. Continuous lines display the theoretical prediction of the Umodel, dotted lines prediction of LQ model for RT and Jung's model for HT. The clonogenic survival curves for 42.5°C and 46.5°C are shown in supplementary Figure SI-1. (c) Advance rate in the SLD chain r , and maximum repair rate q_{max} as functions of the HT temperature for Cal33 cell line. In the inset the difference between the two parameters in linear scale. The behavior of these parameters for the other seven cell lines is shown in supplementary Figure SI-6.

Radiation and hyperthermia monotreatments

A functional model of sequential TRT has to reproduce the survival curves from both mono-treatments individually before applying it to their combination. For ionizing radiation, the LQ model offers one of the best and most robust approaches in predicting the survival fraction as a function of the irradiation dose²⁴. However, the LQ-model parameters (α and β) represent single and double DNA breaks, which do not occur under HT temperatures. Therefore, despite its simplicity and good performance, the LQ model is unsuitable for describing HT survival data. In contrast, Jung's model, based on general SLD accumulation, may thus describe the damage induced by any treatment. This feature of Jung's model has so far not been exploited. Fig. 2(a) presents the survival data and the LQ- and Jung's model predictions for our previously published dataset of eight different HNSCC cell lines treated with X-rays⁶². The Umodel has coefficients of determination slightly higher than the LQ and Jung's -models ($\langle R_{LQ}^2 \rangle = \langle R_{Jung}^2 \rangle = 0.997$, $\langle R_{Umodel}^2 \rangle = 0.999$; see detailed results in Table SI-1).

For the hyperthermia treatment, we experimentally determined the clonogenic survival curves for the eight HNSCC cell lines as a function of HT exposure time at three different temperatures: 42.5 °C, 44.5 °C and 46.5°C (Fig. 2(b), Fig. SI-1). Here, the application of Jung's model shows similar or better performance than the Umodel, except for the UTSCC-14 cell line at 44.5 °C (Table SI-3). UT-SCC-14 cells present a different behavior, as the curve flattens upon longer exposure times (Fig. 2(b)). As detailed below, similar observations come from several independent literature datasets documenting clonogenic survival upon HT treatment.

Furthermore, and as discussed in the methods section, the advance rate r is restricted to grow exponentially with increasing temperature, as predicted by thermodynamics³³. This condition helps the search algorithm improve the fitting in all the cases, reducing the identifiability problem. Accordingly, the maximum regression rate q_{max} is set to follow the same trend as the cell attempts to fix the induced harm. For most of the cell types, the difference between the damage and regression rates increases with temperature and the curves begin to deviate (Fig. 2(c), Fig. SI-6; the q_{max} values are all listed in Table SI-3).

Flattening survival curves and adaptation to treatment

As shown in the previous section, some survival curves have a shape characterized by a reduction of the slope at higher exposure doses. Here, even Jung's model fails to reproduce this type of data. The regression function introduced in the Umodel (Eq. 11) critically improves the capability of the model to describe the referred behavior of the cellular population, such that the Umodel performs better than the LQ and Jung's model in all these cases.

Hyperthermia and thermal-adaptation. When cell cultures under HT become more resistant to increasing thermal dose, the logarithmic clonogenic survival curves start flattening⁷⁰. We call this behavior *adaptation to treatment*. It is cell line-dependent and especially frequent for mild HT. We observed such behavior in our HNSCC models, and similar observations come from several independent literature datasets documenting clonogenic survival upon HT treatment^{29,32,47,63–65}. Here, Jung’s model reaches the limit of a straight line, since does not include possible cell recovery and mitigation of thermal damage. Accordingly, the Umodel predicts clonogenic survival under these circumstances more precisely, as documented in Fig. 3, Fig. SI-2 to SI-5 and Tables SI-IV, SI-V. The corresponding increase of the q_{\max} parameter with temperature is shown in Fig. SI-7 and SI-8; the values are all listed in Table SI-4. We, therefore, hypothesize that cell cultures exposed to moderate HT, particularly around $\approx 43^{\circ}\text{C}$, adapt to the stressful conditions by upregulating survival mechanisms and enhancing recovery. Consequently, the decline in the survival rate slows down as the exposure time increases, and the expected shoulder of the survival curve ($-\ln(S)$) no longer takes place. Several studies have shown that the response to HT is triggered by protein denaturation, where heat shock proteins (HSPs) are activated, and heat shock factors (HSFs) are upregulated in a nonlinear manner^{41–45}. Our work comprises and mathematically simplifies those regulatory mechanisms through a modified Michaelis-Menten model, capable of describing the nonlinear rise of the refolded proteins during the exposure time, as dictated by Eq. 9. Adaptation to treatment is described by introducing the mending rate (Eq. 11) into Jung’s model (Eq. 12).

Irradiation. A meta-study from 2021⁷¹ compared ion beam irradiation with a reference photon irradiation (X-ray), surveying *in vitro* clonogenic cell survival data across the literature. The authors identified several data series showing signs of cell resistance with higher radiation doses, i.e., the linear-quadratic behavior at lower doses transitioning into purely logarithmic or even concave dose-response relationship at higher doses. The straightening survival curve progression is expressed as negative β -values in the LQ model fittings, which contradicts the probabilistic conception of the radiobiological parameters in the LQ model⁷². Indeed, this limitation of the LQ model in the high-dose range has been previously addressed⁷³. We tested the LQ- and U- models in three such datasets extracted from published literature, again finding the Umodel’s superior performance. The results are documented in Fig. 2; Table SI-2 summarizes all parameters and R^2 values.

An early mechanistic interpretation of the high-dose radioresistance phenomenon in single-dose irradiation experiments suggests that cell subpopulations with different sensitivities co-exist. Here, the resistant subpopulations dominate clonogenic survival at higher doses, manifesting a “resistant tail” of the survival curve⁷⁴. The regression rate of the Umodel reflects such scenarios to some extent by encompassing an average upregulation in the DNA repair capacity. A more recent alternative hypothesis by Friedrich et al. suggests a model based on the spatial distribution of the DSBs within a discrete organized chromatin region on a megabase pair scale - a giant loop³⁵). In this case, the deviation from the survival curve at higher radiation doses predicted via the LQ model is attributed to the formation of clustered DNA damage, defined as the mutual effect of DSBs over more considerable genomic distances. The model proposes the highest radiation efficiency if precisely two DSBs are induced within one loop. More than two DSBs on average per loop do not linearly enhance the radiation response. Hence, the relative contribution to lethality per DSB decreases, and a saturation effect occurs³⁶. This phenomenon may explain the lower effectiveness of higher doses as reflected by straight or flattening tails of the survival curves. Such a mechanism is expected to be more critical for high LET/particle irradiation, i.e., the probability of inducing cluster DNA damage is higher than for conventional X-rays³⁶. Variation in the LQ model β values with LET have already been demonstrated^{71,75}. This particular mechanistic link has not been considered in our model. However, the reduced lethality at higher doses can still be modeled as a decreased advance rate r , equivalent to the more effective repair in the Umodel.

Taken together, survival curves that do not conform to the standard LQ model can appear upon HT and irradiation monotherapy. More generalizable mathematical models are thus needed as the underlying phenomena also have profound relevance for treatment planning and prognosis in the clinical setting. Although the investigation of the underlying processes is beyond the scope of this paper, including a regression function between consecutive stages of SLD accumulation makes the Umodel versatile and applicable for any type and shape of leveling clonogenic survival curve.

Combined treatment

The radiosensitizing efficacy of HT has been widely proven in different *in vitro* and *in vivo* models of various normal and cancer cell types^{4,76–80}. Radiosensitization at the cellular level is mainly attributed to the deterioration of the DNA-repair machinery. The proposed Umodel thus contains a regression function, i.e., decreased repair rate of the radiation-induced damage, as emphasized in the Methods section.

$$q_{RT_{new}}(t) = q_{RT_{old}}(t) - q_{red}(t_{HT}, T_{HT}).$$

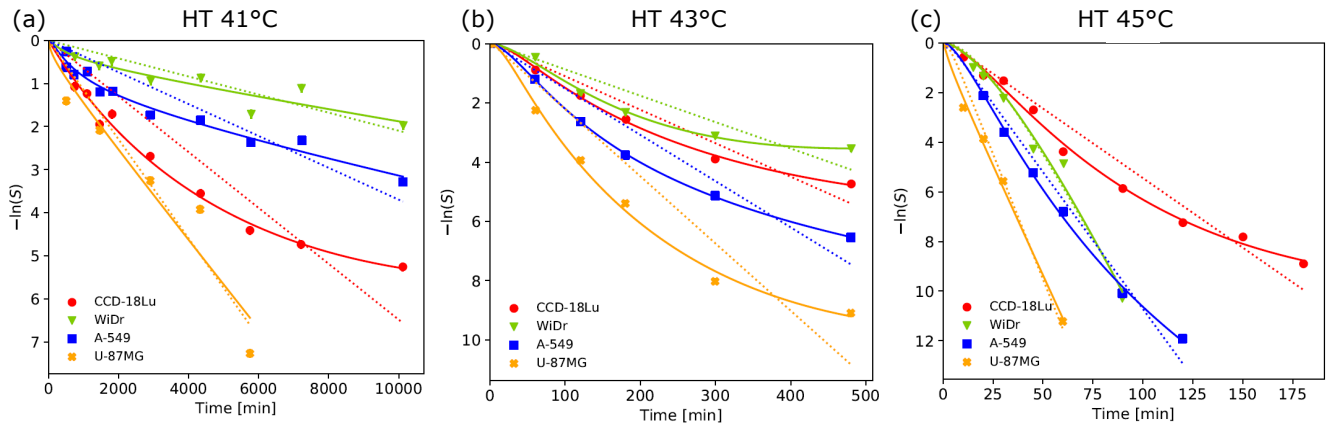


Figure 3. Comparison Jung's and Umodel in HT clonogenic survival experiments that display adaptation to therapy. Symbols represent cell survival fractions ($-\ln(S)$) obtained from clonogenic assays using different human cell models (normal human fibroblasts CCD-18Lu, lung carcinoma A-549, glioblastoma-astrocytoma U-87MG, and colon carcinoma WiDr) exposed to HT at 41°C, 43°C, and 45°C⁶⁵. Continuous lines display the theoretical prediction of the Umodel, and dotted lines of Jung's model.

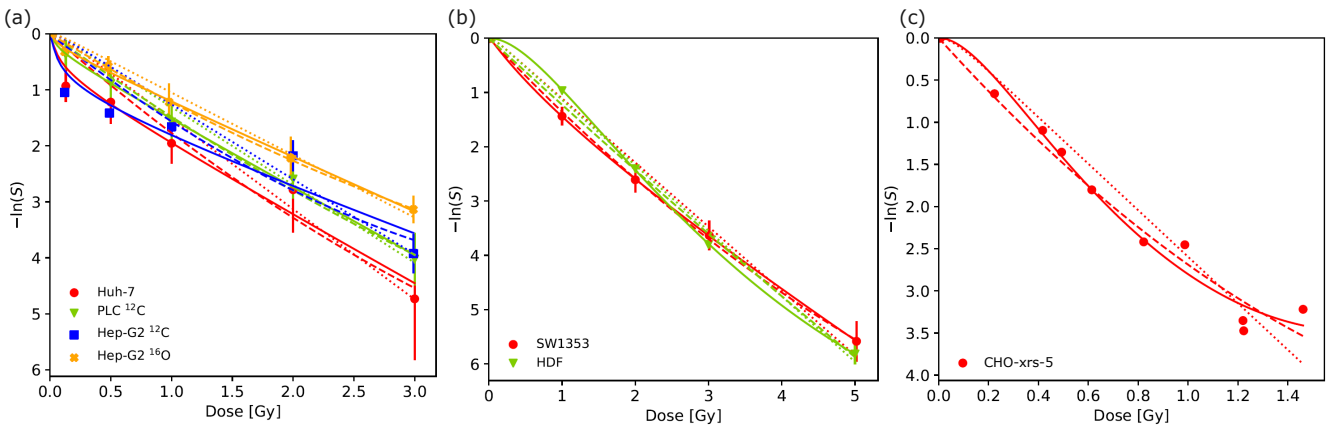


Figure 4. Comparison the LQ and Umodel in clonogenic survival experiments upon particle irradiation that differ from conventional LQ behavior. Symbols represent cell survival fractions ($-\ln(S)$) obtained from clonogenic assays from different human cell types exposed to particle irradiation (a) human hepatocellular carcinomas Huh-7 and PLC and hepatoblastoma HepG2 exposed to carbon ions ^{12}C and hepatoblastoma HepG2 exposed to oxygen ions ^{16}O ⁶⁶, (b), chondrosarcoma SW1353 and normal human dermal fibroblasts HDF exposed to carbon ions ^{12}C ⁶⁷, (c) radiosensitive mutant of Chinese hamster ovary cells CHO-xrs-5 exposed to carbon ions ^{12}C ⁶⁸. Continuous lines display the theoretical prediction of the Umodel, dotted lines of LQ model, and dashed lines of Jung's model.

Jung's and the Umodel were fitted to experimental clonogenic survival data recorded upon combined TRT. FaDu and SAS HNSCC cells were first exposed to three different HT doses (40.5°C, 42.5°C, and 44.5°C for 15-30 minutes) and then immediately exposed to 0 - 6 Gy of X-ray irradiation. Averaged clonogenic survival curves from three independent experiments and the respective model fittings are documented in supplementary Figure SI-9(a-f), showing that the two models yield comparable performance. The models were also applied to fit two additional data sets from literature^{26,69}, with similar results (Figure SI-9(g-k)). Notably, the gap between applications in the combined treatment has effectively been null in all experiments. The thermal enhancement ratios were calculated as a fold change of the advance rate of RT combined with HT $r_{RT_{new}}$ in comparison to the advance rate of RT alone $r_{RT_{old}}$. Hence, as shown in Eqs. 17 and 18 $TER = \frac{r_{RT_{new}}}{r_{RT_{old}}}$. TERs were plotted as a function of exposure time and temperature in Fig. 5; (a,c) for FaDu, (b,d) for SAS and Fig. SI-10 for the literature data. When the TERs are linear functions of the HT treatment time, the slopes display exponential dependencies with HT temperature, as previously found and predicted^{4,33}. All fitting parameters and TER calculations are summarized in Tables SI-VII to SI-X.

With rising temperatures, the model predicts an increase in the SLD rate as expected, but counterintuitively shows a decrease in the damage fixation rate of radiation c_{RT} (Fig. 5(e,f), Fig. SI-10 (e,f)). This observation is difficult to interpret since HT affects different cellular processes, such as proliferation, thermal and ER stress responses, autophagy, regulated cell death pathways, and DNA damage repair. However, proliferative cell death increases with HT treatment time and temperature despite the reduction of c_{RT} in the combined TRT scheme. Accordingly, time in the Umodel is not chronological but is a measure of the applied dose. Therefore, the accumulation of SLD may cause the cell to die (i.e., permanently lose proliferative capacity) whenever r increases and c decreases, even if the process is delayed due to a reduced c . From a mechanistic point of view, it is speculated that the reduction of c_{RT} can be associated with the effects of heat on various cellular processes linked to cell death, for instance - and among other possibilities - (i) the heat-induced denaturation of endonucleases, which are responsible for excising the damaged DNA fragment during the repair of single-strand breaks⁵⁴, (ii) the increased probability of cell cycle arrest that could potentially reduce the rate c_{RT} by delaying cell death⁵⁴, and (iii) the reduction of the available molecular oxygen which is known to be required for the DNA-damage fixation. The latter seems relevant for the *in vitro* response to TRT, while the oxygen supply in the *in vivo* situation is differently and more complexly affected since HT enhances blood flow, thereby improving the tumor and tissue reoxygenation.

Since each therapy fraction is mathematically represented as a treatment operator, the Umodel enables incorporating not only fractions of the individual therapies but also, in the combined scheme, defining and modifying the order of two treatment modalities. The operational nature of Jung's model, and consequently the Umodel allows it to describe sequential treatments of different damage sources and mathematically model additive and synergistic effects. Hence, it can be considered for modeling combination treatment outcomes where radiosensitization was achieved by means other than hyperthermia. For demonstration, we applied the Umodel to selected clonogenic cell survival data from a previously published study of our laboratory, where we combined RT with a metabolic targeting strategy⁶². A panel of HNSCC cell lines was deprived of the proteinogenic amino acid arginine for 24 hours before irradiation. Jung's model and the Umodel fit most of the selected series very well. However, those survival curves that displayed a flattening course at higher radiation doses were reproduced more precisely by the Umodel (Fig. 6). The decrease in the slope could here, indeed, be explained by the presence of subpopulations with different sensitivities and responsiveness to proteogenic and ER stress that can potentially coexist in one cell line. Nonetheless, our fittings to these datasets further demonstrate the versatility of the Umodel for generalizable predictions that do not rely on underlying biological mechanism.

The main limitation of the proposed Umodel is the lack of identifiability of its parameters inherited from Jung's model. Lack of identifiability is quite a common problem in mathematical models and is receiving increasing attention in the applied mathematics community⁵⁸⁻⁶⁰. It follows from the fact that some parameters correlate with each other, and therefore, different sets of parameter values lead to very similar goodness-of-fit within the uncertainty of the experimental data. This flaw in the model hinders the interpretation of the specific parameter values and their association with the sensitivity of different cell types to treatment. Consequently, in this paper, we can describe trends of the parameters as a function of thermal or radiation dose but not yet the biological meaning of the specific parameter values.

Nevertheless, the parameter trends can provide more insights into the underlying phenomena because they come from simultaneous fitting to several independent data sets. One way to improve the identifiability is to restrict the multiparametric space, as we have done by introducing thermodynamic conditions for the dependence of the model parameters on HT exposure time and temperature. However, the problem still needs to be fully solved; more specific experimental data describing DNA damage and repair would be helpful to validate our current predictions and define a reasonable physiological range for the parameters, improving their identifiability. For instance, extensive experimental quantification of enzyme activities relevant to

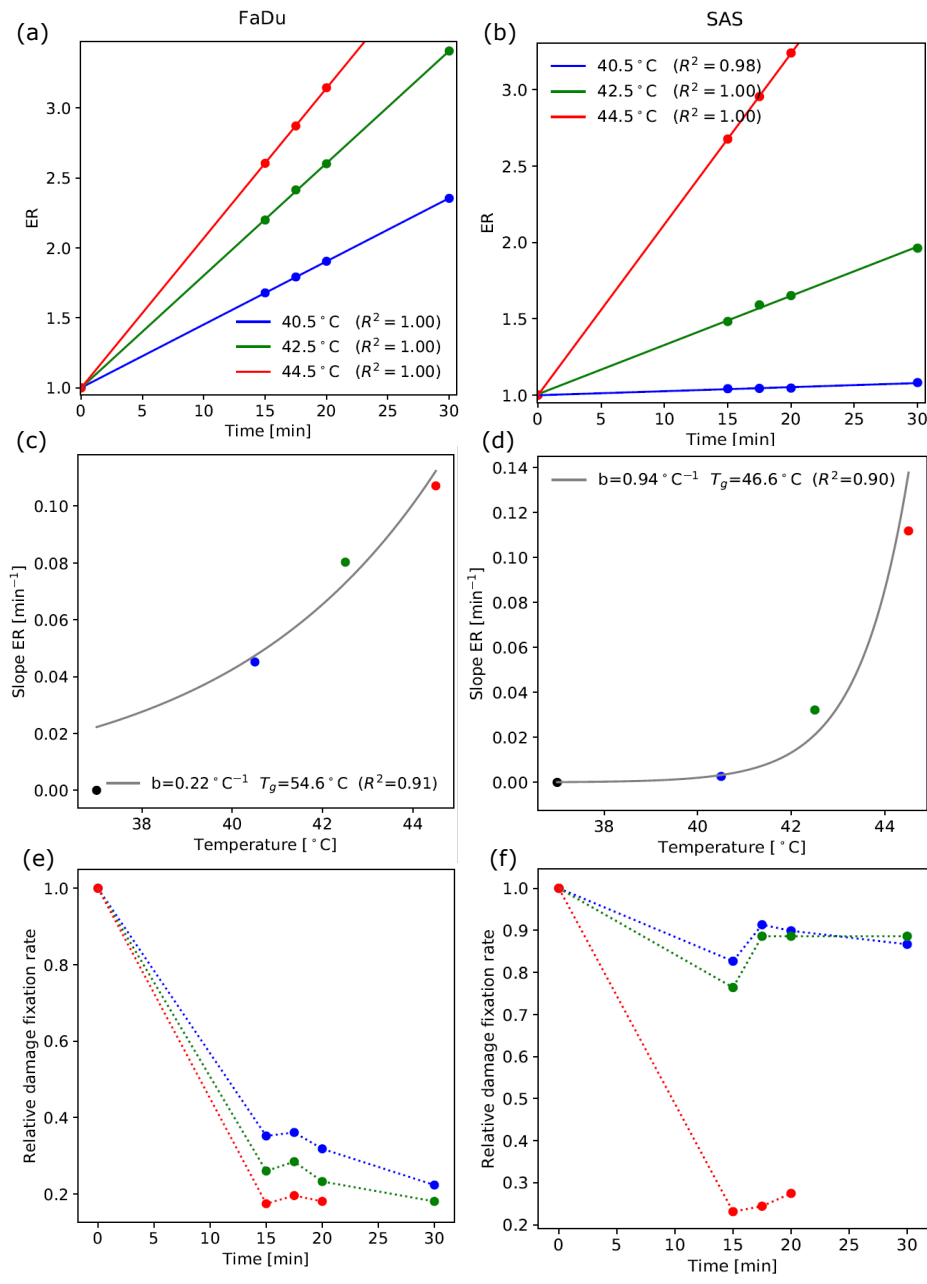


Figure 5. Enhancement of radiation response by HT as a function of exposure time and temperature. (a,b) Linear dependency of the enhancement ratios (ER) with HT exposure time (calculated from Eqs. 17 and 18). (c,d) Slopes from (a) and (b) respectively, as a function of HT temperature. (e,f) Relative damage fixation rate $C_{RT_{new}}/C_{RT_{old}}$ as function of the HT exposure time.

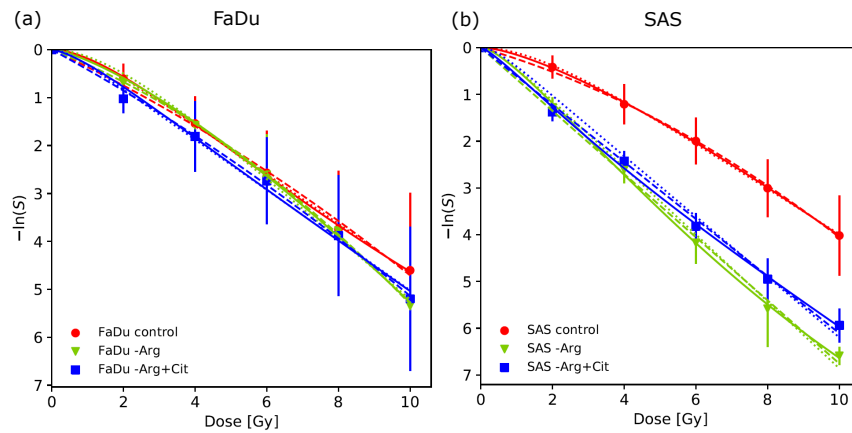


Figure 6. Umodel fittings in clonogenic survival experiments upon metabolic deprivation. Symbols represent cell survival fractions ($-\ln(S)$) obtained from clonogenic assays from (a) FaDu and (b) SAS HNSCC cell lines exposed to different variations of metabolic deprivation followed by 0-8 Gy of irradiation⁶².

DNA repair or protein refolding upon treatment would help to refine the proposed model regarding its biological relevance and robust interpretability.

Conclusions and Outlook

In this work, we extended Jung's model, which originally describes clonogenic cell survival after HT, to various combinatorial treatment approaches and incorporated adaptation to therapy. Due to its compartmental structure, the developed unified model (Umodel) allows the accumulation of SLD without assuming or excluding any particular mechanism of injury. This feature and its mathematical formulation make the model suitable to describe/predict the therapeutic outcome of the individual treatments and their synergistic combination under various scheduling regimes. Since our model is based on the accumulation of non-lethal damage, it also naturally allows the inclusion of prosurvival mechanisms, modeled as an effective enzymatic reaction. This characteristic is highly relevant to describe (plastic) tumor cells that can adapt to treatment, e.g., some cell subpopulations under selected radiation treatments or mild hyperthermia. Our model of enzymatic restoration of damaged molecules contains several simplifications encompassing different processes such as DNA repair, protein refolding, or subpopulation screening. Through this effective enzymatic reaction, we reduced the complexity involved in the actual cellular population responses, being able to modulate and predict atypical average responses of the cell populations with only two adjustable parameters.

We successfully applied the model to several data sets for both treatments, individually as monotherapy or sequentially as a combinatorial approach. Our results show excellent agreement, especially in cases presenting adaptation to treatment, where other models typically fail. The Umodel is, in its nature, capable of including treatment order and interval between the individual modalities and fractionated schemes. This vital attribute encompasses the non-commutative character of sequentially combined TRT. Since the Umodel is based on general thermodynamics and biochemical principles, it contributes to a better understanding of the synergy between HT and radiation beyond the empirical fittings of experimental data. Moreover, its features further grant the model predicting power to other state-of-the-art multimodal approaches combining two or more oncological treatments for better therapeutic results.

The Umodel describes effects as damage accumulation and death in cell cultures as a function of the heat or radiation dose, assessed by treatment time or fixed dose rates. Future extensions of the model could incorporate chronological time. For calibration, this requires additional analytical endpoints of cell damage and death after treatment, which can be monitored over time, such as DNA damage and repair or factors reflecting regulated and non-regulated cell death processes. Therefore, the Umodel represents a starting point for the design and implementation of more in-depth experiments on the synergistic effects between treatment modalities (such as TRT), and it also supports the clinical translation of general model-based survival predictions. Moreover, our model can be directly incorporated into more complex mathematical models of multicellular dynamics, such as tumor spheroids under treatment⁸¹.

Authors contributions

A.M.D.M. conceived the presented idea and developed the theory. S.M. and L.A.K-S designed and supervised the experiments. S.M. and L.E. performed the experiments. A.M.D.M., P.S.C, S.L., and A.G.M. performed the numerical calculations and analyses. All authors contributed to the interpretation of the results. A.M.D.M., S.M., S.L., and L.A.K-S designed and wrote the manuscript. L.A.K-S. supervised the project

Acknowledgments

This work was supported by the German Federal Ministry of Education and Research (BMBF; 03Z1N512; 16dkwn001). We thank Marit Wondrak for technical support of the biological experiments and Damian D. McLeod for helpful discussion.

References

1. Chandra, R. A., Keane, F. K., Voncken, F. E. M. & Thomas, C. R. Contemporary radiotherapy present and future. *The Lancet* **398**, DOI: [https://doi.org/10.1016/S0140-6736\(21\)00233-6](https://doi.org/10.1016/S0140-6736(21)00233-6) (2021).
2. Begg, A. C., Stewart, F. A. & Vens, C. Strategies to improve radiotherapy with targeted drugs. *Nat. Rev. Cancer* **11**, 239–253, DOI: <https://doi.org/10.1038/nrc3007> (2011).
3. Overgaard, J. The heat is (still) on: The past and future of hyperthermic radiation oncology. *Radiother. Oncol.* **109**, 185–187, DOI: <https://doi.org/10.1016/j.radonc.2013.11.004> (2013).
4. Overgaard, J. Simultaneous and sequential hyperthermia and radiation treatment of an experimental tumor and surrounding normal tissue in vivo. *Int. J. Radiat. Oncol.* **6**, 1507–1517, DOI: [https://doi.org/10.1016/0360-3016\(80\)90008-5](https://doi.org/10.1016/0360-3016(80)90008-5) (1980).
5. Mei, X. *et al.* Radiosensitization by hyperthermia: The effects of temperature, sequence, and time interval in cervical cell lines. *Cancers* **12**, DOI: <https://doi.org/10.3390/cancers12030582> (2020).
6. Elming, P. B. *et al.* Hyperthermia: The optimal treatment to overcome radiation resistant hypoxia. *Cancers* **11**, DOI: <https://doi.org/10.3390/cancers11010060> (2019).
7. van Leeuwen, C. M. *et al.* The effect of time interval between radiotherapy and hyperthermia on planned equivalent radiation dose. *Int. J. Hyperth.* **34**, 901–909, DOI: <https://doi.org/10.1080/02656736.2018.1468930> (2018).
8. van Leeuwen, C. M. *et al.* A short time interval between radiotherapy and hyperthermia reduces in-field recurrence and mortality in women with advanced cervical cancer. *Radiat. Oncol.* **12**, 1–8, DOI: <https://doi.org/10.1186/s13014-017-0813-0> (2017).
9. Datta, N. R., Kok, H. P., Crezee, H., Gaip, U. S. & Bodis, S. Integrating loco-hyperthermia into the current oncology practice: Swot and tows analyses. *Front. Oncol.* **10**, 1–30, DOI: <https://doi.org/10.3389/fonc.2020.00819> (2020).
10. Spirou, S. V., Basini, M., Lascialfari, A., Sangregorio, C. & Innocenti, C. Magnetic hyperthermia and radiation therapy: Radiobiological principles and current practice. *Nanomaterials* **8**, 1–22, DOI: <https://doi.org/10.3390/nano8060401> (2018).
11. Moros, E. G., Peñagaricano, J., Novák, P., Straube, W. L. & Myerson, R. J. Present and future technology for simultaneous superficial thermoradiotherapy of breast cancer. *Int. J. Hyperth.* **26**, 699–709, DOI: <https://doi.org/10.3109/02656736.2010.493915> (2010).
12. Scopus database. 579 publications in the last five years. Keywords: Clinical AND Radiation AND Hyperthermia. Accessed: Jan-11-2024.
13. Clinicaltrials. <http://ClinicalTrials.gov>. 45 clinical trials reported active or completed cancer treatment with hyperthermia and radiation. Accessed: Jan-01-2024.
14. Kok, H. P. *et al.* Heating technology for malignant tumors a review. *Int. J. Hyperth.* **37**, 711–741, DOI: <https://doi.org/10.1080/02656736.2020.1779357> (2020).
15. Georgios P. Skandalakis, C. D. R. A. B. J. G. J. R. D. B., Daniel R. Rivera & Hadjipanayis, C. G. Hyperthermia treatment advances for brain tumors. *Int. J. Hyperth.* **37**, 3–19, DOI: <https://doi.org/10.1080/02656736.2020.1772512> (2020).
16. Schupper, A. J., Chanenchuk, T., Racanelli, A., Price, G. & Hadjipanayis, C. G. Laser hyperthermia: Past, present, and future. *Neuro-Oncology* **24**, S42–S51, DOI: <https://doi.org/10.1093/neuonc/noac208> (2022).
17. lian, Y. *et al.* Recent advances on the magnetic nanoparticle-based nanocomposites for magnetic induction hyperthermia of tumor: a short review. *Adv. Compos. Hybrid Mater.* **4**, 925–937, DOI: <https://doi.org/10.1007/s42114-021-00373-3> (2021).
18. Cheng, Y. *et al.* The role of hyperthermia in the multidisciplinary treatment of malignant tumors. *Integr. cancer therapies* **18**, 1–11, DOI: <https://doi.org/10.1177/1534735419876345> (2019).

19. Paulides, M. M., Verduijn, G. M. & Van Holthe, N. Status quo and directions in deep head and neck hyperthermia. *Radiat. Oncol.* **11**, 1–14, DOI: <https://doi.org/10.1186/s13014-016-0588-8> (2016).
20. Kang, J. K. *et al.* Principles and applications of nanomaterial-based hyperthermia in cancer therapy. *Arch. Pharmacol. Res.* **43**, 46–57, DOI: <https://doi.org/10.1007/s12272-020-01206-5> (2020).
21. Hillen, T., de Vries, G., Gong, J. & Finlay, C. From cell population models to tumor control probability: Including cell cycle effects. *Acta Oncol.* **49**, 1315–1323, DOI: <https://doi.org/10.3109/02841861003631487> (2010).
22. Naqa, I. E. *et al.* Datamining approaches for modeling tumor control probability. *Acta Oncol.* **49**, 1363–1373, DOI: <https://doi.org/10.3109/02841861003649224> (2010).
23. Borkenstein, K., Levegrün, S. & Peschke, P. Modeling and computer simulations of tumor growth and tumor response to radiotherapy. *Radiat. Res.* **162**, 71–83, DOI: <https://doi.org/10.1667/RR3193> (2004).
24. Brenner, H. J. & Yerushalmi, A. Combined local hyperthermia and x-irradiation in the treatment of metastatic tumours. *Br. J. Cancer* **33**, 91–95, DOI: <https://doi.org/10.1038/bjc.1976.9> (1975).
25. McMahon, S. J., Schuemann, J., Paganetti, H. & Prise, K. M. Mechanistic modelling of dna repair and cellular survival following radiation-induced dna damage. *Sci. Reports* **6:33290**, 1 – 14, DOI: <https://doi.org/10.1038/srep33290> (2016).
26. Brüningk, S. C. *et al.* A comprehensive model for heat-induced radio-sensitisation. *Int. J. Hyperth.* **34**, 392–402, DOI: <https://doi.org/10.1080/02656736.2017.1341059> (2018). PMID: 28641499.
27. Park, C., Papiez, L., Zhang, S., Story, M. & Timmerman, R. D. Universal survival curve and single fraction equivalent dose: useful tools in understanding potency of ablative radiotherapy. *Int. journal radiation oncology, biology, physics* **71**, 847–852, DOI: <https://doi.org/10.1016/j.ijrobp.2007.10.059> (2008).
28. Pearce, J. A. Comparative analysis of mathematical models of cell death and thermal damage processes. *Int. J. Hyperth.* **29**, 262–280, DOI: <https://doi.org/10.3109/02656736.2013.786140> (2013).
29. Jung, H. A generalized concept for cell killing by heat. *Radiat. Res.* **106**, 56–72, DOI: <https://www.jstor.org/stable/3576561> (1986).
30. Roti, J. L. R. Cellular responses to hyperthermia (40–46°C): Cell killing and molecular events. *Int. J. Hyperth.* **24**, 3–15, DOI: <https://doi.org/10.1080/02656730701769841> (2008).
31. Uchida, N., Kato, H. & Ishida, T. A model for cell killing by continuous heating. *Med. Hypotheses* **41**, 548–553, DOI: [https://doi.org/10.1016/0306-9877\(93\)90112-4](https://doi.org/10.1016/0306-9877(93)90112-4) (1993).
32. Mackey, M. A. & Roti-Roti, J. L. A model of heat-induced clonogenic cell death. *J. Theor. Biol.* **156**, 133–146, DOI: [https://doi.org/10.1016/S0022-5193\(05\)80669-1](https://doi.org/10.1016/S0022-5193(05)80669-1) (1992).
33. De Mendoza, A. M. *et al.* Mathematical model for the thermal enhancement of radiation response: thermodynamic approach. *Sci. Reports* **11**, 1 – 14, DOI: <https://doi.org/10.1038/s41598-021-84620-z> (2021).
34. Tobias, C. A. The repair-misrepair model radiobiology: comparison to other models. *Radiat. Res.* **104**, 77–95, DOI: <https://doi.org/10.2307/3576635> (1985).
35. Friedrich, S. U. D. M., Thomas & Scholz, M. Calculation of the biological effects of ion beams based on the microscopic spatial damage distribution pattern. *Int. J. Radiat. Biol.* **88**, 103–107, DOI: <https://doi.org/10.3109/09553002.2011.611213> (2012).
36. Friedrich, T., Durante, M. & Scholz, M. Modeling cell survival after photon irradiation based on double-strand break clustering in megabase pair chromatin loops. *Radiat. Res.* **178**, 385–394, DOI: <https://doi.org/10.1667/RR2964.1> (2012).
37. Frankenberg-Schwager, M. Review of repair kinetics for dna damage induced in eukaryotic cells in vitro by ionizing radiation. *Radiother. Oncol.* **14**, 307–320, DOI: [https://doi.org/10.1016/0167-8140\(89\)90143-6](https://doi.org/10.1016/0167-8140(89)90143-6) (1989).
38. Alberts, B. *et al.* *Molecular Biology of the Cell* (Garland, 2002), 4th edn.
39. Hall, E. J. & Giaccia, A. J. *Radiobiology for the radiologist* (Lippincott Williams and Wilkins, 2012), 7 edn.
40. Crooke, P. S. & Parl, F. F. A mathematical model for dna and repair. *J. Nucleic Acids Special issue: DNA Damage, Mutagenesis, and DNA Repair*, 1 – 7, DOI: <https://doi.org/10.4061/2010/352603> (2010).
41. Zheng, X. *et al.* Dynamic control of hsf1 during heat shock by a chaperone switch and phosphorylation. *eLife* **5**, e18638, DOI: <https://doi.org/10.7554/eLife.18638> (2016).
42. Ladjimi, M. T. *et al.* Dynamical thermal dose models and dose time-profile effects. *Int. J. Hyperth.* **36**, 720–728, DOI: <https://doi.org/10.1080/02656736.2019.1633478> (2019). PMID: 31353987.

43. Sivéry, A., Courtade, E. & Thommen, Q. A minimal titration model of mammalian dynamical heat shock response. *Phys. Biol.* **13**, 066008, DOI: <https://doi.org/10.1088/1478-3975/13/6/066008> (2016).
44. Scheff, J. D., Stallings, J. D., Reifman, J. & Rakesh, V. Mathematical modeling of the heat-shock response in hela cells. *Biophys. J.* **109**, 182 – 193, DOI: <https://doi.org/10.1016/j.bpj.2015.06.027> (2015).
45. Peper, A., Grimbergen, C. A., Spaan, J. A. E., Souren, J. E. M. & Van Wijk, R. A mathematical model of the hsp70 regulation in the cell. *Int. J. Hyperth.* **14**, 97–124, DOI: <https://doi.org/10.3109/02656739809018218> (1998). PMID: 9483450.
46. Roskoski, R. Michaelis-menten kinetics. In *Reference Module in Biomedical Sciences*, DOI: <https://doi.org/10.1016/B978-0-12-801238-3.05143-6> (Elsevier, 2015).
47. Sapareto, S. A. *et al.* Effects of Hyperthermia on Survival and Progression of Chinese Hamster Ovary Cells. *Cancer Res.* **38**, 393–400, DOI: <http://cancerres.aacrjournals.org/content/38/2/393> (1978).
48. Lindegaard, J. C. & Overgaard, J. Step-down heating in a c3h mammary carcinoma in vivo: Effects of varying the time and temperature of the sensitizing treatment. *Int. J. Hyperth.* **6**, 607–617, DOI: <https://doi.org/10.3109/02656739009140957> (1990).
49. Lindegaard, J. C. & Overgaard, J. Effect of step-down heating on hyperthermic radiosensitization in an experimental tumor and a normal tissue in vivo. *Radiother. oncology : journal Eur. Soc. for Ther. Radiol. Oncol.* **11**, 143–151, DOI: [https://doi.org/10.1016/0167-8140\(88\)90250-2](https://doi.org/10.1016/0167-8140(88)90250-2) (1988).
50. Lindegaard, J. C. Winner of the lund science 1992 thermosensitization induced by step-down heating: A review on heat-induced sensitization to hyperthermia alone or hyperthermia combined with radiation. *Int. J. Hyperth.* **8**, 561–586, DOI: <https://doi.org/10.3109/02656739209037994> (1992).
51. Lindegaard, J. & Overgaard, J. Effect of step-down heating on hyperthermic radiosensitization in an experimental tumor and a normal tissue in vivo. *Radiother. Oncol.* **11**, 143–151, DOI: [https://doi.org/10.1016/0167-8140\(88\)90250-2](https://doi.org/10.1016/0167-8140(88)90250-2) (1988).
52. McMahon, S. J. & Prise, K. M. A mechanistic dna repair and survival model (medras): Applications to intrinsic radiosensitivity, relative biological effectiveness and dose-rate. *Front. Oncol.* **11**, DOI: <https://doi.org/10.3389/fonc.2021.689112> (2021).
53. Karschau, J. *et al.* A matter of life or death: Modeling dna damage and repair in bacteria. *Biophys. J.* **100**, 814 – 821, DOI: <https://doi.org/10.1016/j.bpj.2010.12.3713> (2011).
54. Oei, A. L., Vriend, L. E. M., Crezee, J., Franken, N. A. P. & Krawczyk, P. M. Effects of hyperthermia on DNA repair pathways: one treatment to inhibit them all. *Radiat. Oncol.* **165**, DOI: <https://doi.org/10.1186/s13014-015-0462-0> (2015).
55. Newville, M., Stensitzki, T., Allen, D. B. & Ingargiola, A. Lmfit: Non-linear least-square minimization and curve-fitting for python, DOI: <https://doi.org/10.5281/zenodo.11813> (2014).
56. Levenberg, K. A method for the solution of certain non-linear problems in least squares. *Q. Appl. Math.* **2**, 164–168, DOI: <https://doi.org/10.1090/qam/10666> (1944).
57. Marquardt, D. W. An algorithm for least-squares estimation of nonlinear parameters. *J. Soc. for Ind. Appl. Math.* **11**, 431–441, DOI: <https://doi.org/10.1137/0111030> (1963).
58. Wu, Z., Phan, T., Baez, J., Kuang, Y. & Kostelich, E. J. Predictability and identifiability assessment of models for prostate cancer under androgen suppression therapy. *Math. Biosci. Eng.* **16**, 3512–3536, DOI: <https://doi.org/10.3934/mbe.2019176> (2019).
59. Muñoz-Tamayo, R. *et al.* Review: To be or not to be an identifiable model. is this a relevant question in animal science modelling? *animal* **12**, 701–712, DOI: <https://doi.org/10.1017/S1751731117002774> (2018).
60. Alahmadi, A. *et al.* Influencing public health with data-informed mathematical models of infectious diseases: Recent developments and new challenges. *Epidemics* **32**, 100393, DOI: <https://doi.org/10.1016/j.epidem.2020.100393> (2020).
61. Eichel, W., Zips, D., Dörfler, A., Grénman, R. & Baumann, M. Splicing mutations in tp53 in human squamous cell carcinoma lines influence immunohistochemical detection. *J. Histochem. Cytochem.* **50**, 197–204, DOI: <https://doi.org/10.1177/002215540205000207> (2002).
62. Chen, O. *et al.* Dual role of er stress in response to metabolic co-targeting and radiosensitivity in head and neck cancer cells. *Cell. Mol. Life Sci.* **78**, 3021–3044, DOI: <https://doi.org/10.1007/s00018-020-03704-7> (2021).
63. Gerner, E. W. Thermal dose and time-temperature factors for biological responses to heat shock. *Int. J. Hyperth.* **3**, 319–327, DOI: <https://doi.org/10.3109/02656738709140402> (1987).

64. Oñara, M. D., Xiong, Q. B., Boyer, J. W. & Leeper, D. B. Intrinsic thermal response, thermotolerance development and stepdown heating in murine bone marrow progenitor cells. *Int. J. Hyperth.* **8**, 451–461, DOI: <https://doi.org/10.3109/02656739209037983> (1992).
65. Armour, E. P., McEachern, D., Wang, Z., Corry, P. M. & Martinez, A. Sensitivity of Human Cells to Mild Hyperthermia. *Cancer Res.* **53**, 2740–2744, DOI: <https://aacrjournals.org/cancerres/article/53/12/2740/498879/Sensitivity-of-Human-Cells-to-Mild-Hyperthermia1> (1993).
66. Habermehl, D. *et al.* The relative effectiveness for carbon and oxygen ion beams using the raster-scanning technique in hepatocellular carcinoma cell lines. *PLOS ONE* **9**, 1–10, DOI: <https://doi.org/10.1371/journal.pone.0113591> (2014).
67. Yagi, M. *et al.* A consistent protocol reveals a large heterogeneity in the biological effectiveness of proton and carbon-ion beams for various sarcoma and normal-tissue-derived cell lines. *Cancers* **14**, 1–12, DOI: <https://doi.org/10.3390/cancers14082009> (2009).
68. Weyrather, W. K., Ritter, S., Scholz, M. & Kraft, G. Rbe for carbon track-segment irradiation in cell lines of differing repair capacity. *Int. J. Radiat. Biol.* **75**, 1357–1364, DOI: <https://doi.org/10.1080/095530099139232> (1999).
69. Dikomey, E. & Jung, H. W. Thermal radiosensitization in cho cells by prior heating at 41–46 °c. *Int. journal radiation biology* **59**, 815–25, DOI: <https://doi.org/10.1080/09553009114550711> (1991).
70. Dewey, W. C. Interaction of heat with radiation and chemotherapy. *Cancer Res.* **44**, 4714s–4720s (1984).
71. Friedrich, T., Pfuhl, T. & Scholz, M. Update of the particle irradiation data ensemble (pide) for cell survival. *J. Radiat. Res.* **62**, 645–655, DOI: <https://doi.org/10.1093/jrr/rrab034> (2021).
72. Chadwick, K. H. & Leenhouts, H. P. A molecular theory of cell survival. *Phys. Medicine Biol.* **18**, 78–87, DOI: <https://doi.org/10.1088/0031-9155/18/1/007> (1973).
73. Schlesinger, D. *et al.* Equivalence of cell survival data for radiation dose and thermal dose in ablative treatments: analysis applied to essential tremor thalamotomy by focused ultrasound and gamma knife. *Int. journal hyperthermia* **33**, 401–410, DOI: <https://doi.org/10.1080/02656736.2016.1278281> (2017).
74. Denekamp, J., Whitmore, G. & Jeggo, P. Biphasic survival curves for xrs radiosensitive cells: subpopulations or transient expression of repair competence? *Int. journal radiation biology* **55**, 605–617, DOI: <https://doi.org/10.1080/09553008914550651> (1989).
75. Friedrich, T., Scholz, U., Elsässer, T., Durante, M. & Scholz, M. Systematic analysis of rbe and related quantities using a database of cell survival experiments with ion beam irradiation. *J. Radiat. Res.* **54**, 494–514, DOI: <https://doi.org/10.1093/jrr/rrs114> (2012).
76. Vujaskovic, Z. & Song, C. W. Physiological mechanisms underlying heat-induced radiosensitization. *Int. J. Hyperth.* **20**, 163–174, DOI: <https://doi.org/10.1080/02656730310001619514> (2004).
77. Konings, A. W. T. *Interaction of Heat and Radiation In Vitro and In Vivo*, 89–102 (Springer Berlin Heidelberg, 1995).
78. Oei, A. *et al.* Molecular and biological rationale of hyperthermia as radio- and chemosensitizer. *Adv. Drug Deliv. Rev.* **163-164**, 84–97, DOI: <https://doi.org/10.1016/j.addr.2020.01.003> (2020).
79. Brüningk, S. C., Ziegenhein, P., Rivens, I., Oelfke, U. & Haar, G. t. A cellular automaton model for spheroid response to radiation and hyperthermia treatments. *Sci. Reports* **9**, 17674, DOI: <https://doi.org/10.1038/s41598-019-54117-x> (2019).
80. Chen, O. *et al.* Efficient heat shock response affects hyperthermia-induced radiosensitization in a tumor spheroid control probability assay. *Cancers* **13**, 3168, DOI: <https://doi.org/10.3390/cancers13133168> (2021).
81. Franke, F. *et al.* Efficient radial-shell model for 3d tumor spheroid dynamics with radiotherapy. *Cancers* **15(23)**,5345,DOI: <https://doi.org/10.3390/cancers15235645> (2023).
82. Magnus, W. On the solution of differential equations for a linear operator. *Commun. on Pure Appl. Math.* **7**, 649, DOI: <https://doi.org/https://doi.org/10.1002/cpa.3160070404> (1954).

Supplemental Information

1 Repair rate dependent on n

When an n -dependent repair rate q_n is included into the model, the net advance rate $r_n = p - q_n$ changes with the level of SLD. The probability that the cell is in the n -th compartment is given by the solution of the modified balance equation

$$\frac{dP_n(t)}{dt} = -r_n P_n(t) - nc P_n(t) + r_{n-1} P_{n-1}(t), \quad (20)$$

Since the rates r and c are not time-dependent, the evolution of the state vector can be written as $\frac{d\vec{P}(t)}{dt} = \hat{A}\vec{P}(t)$. The elements of the transition matrix \hat{A}_{ij} define the influx rate from $n = j$ to $n = i$, and the diagonal elements \hat{A}_{ii} are the net flux at each stage. The general solution of Eq.20 is $\vec{P}(t) = e^{\hat{A}t}\vec{P}(t=0)$, which can be written for the n -th element as

$$P_n(t) = \left(\prod_{i=0}^{n-1} r_i \right) \sum_{i=0}^n \frac{(-1)^i e^{-Y_i t}}{\prod_{j=0}^{i-1} F_{j,i} \prod_{j=i+1}^n F_{i,j}} \quad (21)$$

with $Y_n = nc + r_n$, and $F_{k,l} = \begin{cases} 1 & \text{if } k \geq l \\ Y_l - Y_k & \text{otherwise.} \end{cases}$

The survival probability is equal to the probability of being at any of the non-lethal damage compartments $S(t) = \sum_{n=0}^{\infty} P(n, t)$. In the case without repair ($q_n = 0$ and $r_n \rightarrow r$) the original Jung's model is recovered and the survival probability reads $S(t) = \exp\left\{\frac{r}{c}[1 - ct - e^{-ct}]\right\}$. When repair is included in the Jung's model (eq. 21), it is not possible to obtain a closed exponential for the survival probability. Instead, we assume that the cell goes through a maximum number of possible nonlethal lesions n_{max} and calculate numerically:

$$S(t) = \sum_{n=0}^{n_{max}} P(n, t) \quad (22)$$

We proposed and tried three different functional forms for the repair function:

$$q_n = r \left(\frac{n - n_{max}}{n_{max}} \right), \quad (23)$$

$$q_n = q/n, \quad (24)$$

$$q_n = \frac{qn}{k+n}. \quad (25)$$

Equation 23 describes a linear raise of the repair as a function of the damage stage n . Equation 24 describes a non-linear decay with an additional adjustable parameter q . Equation 25 describes a possible sigmoidal up-regulation of repair when the sublethal damage (SLD) increases. The results (not presented) showed no improvement over the original Jung's model.

2 Approximation in the Magnus series

For the case where the sublethal damage accumulation rate r is time dependent, the transition matrix \hat{A} becomes time-dependent too and then we aim to solve

$$\frac{d\vec{P}(t)}{dt} = \hat{A}(t)\vec{P} \quad (26)$$

for the initial condition $\vec{P}(0) = (1, 0, 0, \dots, 0)^T$, where the superscript T denotes the transpose of a matrix. This initial condition indicates that just at the beginning of the treatment, all the cellular population is at the $n = 0$ compartment, meaning that no damage has been inflicted yet. However, the solution $\vec{P}(t) = e^{\int_0^t \hat{A}(t) dt} \vec{P}(0)$ does not hold any more, and one needs to be careful

because the transition matrix \hat{A} is now a function of time. This implies that the matrix does not commute when it is evaluated at different times $[\hat{A}(t_i), \hat{A}(t_j)] = \hat{A}(t_i) \cdot \hat{A}(t_j) - \hat{A}(t_j) \cdot \hat{A}(t_i) \neq 0$.

The solution to this initial-value problem was introduced by Magnus⁸², expressing the solution through the exponential of a certain $n \times n$ matrix $\hat{\Omega}(t)$:

$$\vec{P}(t) = e^{\hat{\Omega}(t)} \vec{P}(0), \quad (27)$$

where $\hat{\Omega}(t)$ is subsequently constructed as a series expansion $\hat{\Omega}(t) = \sum_{k=1}^{\infty} \hat{\Omega}_k(t)$, with

$$\begin{aligned} \hat{\Omega}_1(t) &= \int_0^t A(t_1) dt_1, \\ \hat{\Omega}_2(t) &= \frac{1}{2} \int_0^t dt_1 \int_0^{t_1} dt_2 [A(t_1), A(t_2)], \\ \hat{\Omega}_3(t) &= \frac{1}{6} \int_0^t dt_1 \int_0^{t_1} dt_2 \int_0^{t_2} dt_3 ([A(t_1), [A(t_2), A(t_3)]] + [A(t_3), [A(t_2), A(t_1)]]), \\ \hat{\Omega}_4(t) &= \frac{1}{12} \int_0^t dt_1 \int_0^{t_1} dt_2 \int_0^{t_2} dt_3 \int_0^{t_3} dt_4 ([[A_1, A_2], A_3], A_4] \\ &\quad + [A_1, [[A_2, A_3], A_4]] + [A_1, [A_2, [A_3, A_4]]] + [A_2, [A_3, [A_4, A_1]]]), \\ &\vdots \end{aligned}$$

Keeping $\hat{\Omega}(t)$ to first order in the expansion is a valid approximation when the parameters are approximately constant for the most of the treatment time. Then, the approximated solution of Eq. 26 would be again

$$\vec{P}(t) \approx e^{\int_0^t \hat{A}(t) dt} \vec{P}(0).$$

Since higher order terms become smaller, we estimate the error as the difference of between the second and the first order contributions:

$$\epsilon = e^{\hat{\Omega}_1(t) + \hat{\Omega}_2(t)} \vec{P}(0) - e^{\hat{\Omega}_1(t)} \vec{P}(0). \quad (28)$$

As an example, we calculate the error for the parameters obtained for UT-SCC-14 cell line under 45°C HT, because it is the only case in our experiments displaying adaptation to treatment, and therefore, a time-dependent rate of SLD accumulation. At $t = 1$ min, this error range below 10^{-4} ; and below 10^{-46} at $t = 60$ min. The parameters used for this results are reported in Table 3

3 Time lapse between sequential treatments

In sequential thermoradiotherapy experiments, there is usually a time elapsed between the administration of the individual modalities. Early experiments showed that in the sequential application of HT and RT, the synergistic outcome is affected not only by the order of application, but also by the time lapse (gap) between the treatments^{4,50}. In our model, the recovery processes activated during the first treatment, modify the final outcome and lower the synergy of the combined treatment. Hence, we included of a ‘‘gap’’ operator \hat{A}_{t_g} between \hat{A}_{t_1} and \hat{A}_{t_2} , which enables the description of this realistic situation. The total outcome for the cellular state is represented by

$$\vec{P}(t_1, t_g, t_2) = e^{\hat{A}_{t_2}} e^{\hat{A}_{t_g}} e^{\hat{A}_{t_1}} \vec{P}(0). \quad (29)$$

Here t_g is the gap between treatments 1 and 2, \hat{A}_{t_g} is given by Eqs. 4 and 6 in the main text, with gap parameters $r_g = c_g = 0$, and $q_g(t)$. The latter is correlated to the regression (recovery rate of the first treatment, which has to be calibrated with survival data for sequential TRT with varying gaps.

4 Radiation treatment results

The Umodel parameters (r, c, q_{max} and k) are presented in Table 1 for the head and neck squamous cell carcinoma (HNSCC) cell lines from our experiments, with the respective goodness of the fit (R^2) of the LQ model and Jung's model for comparison. In most cases, the Umodel performs better or similarly because the logarithmic survival curves ($-\ln(S)$) do not display adaptation to treatment (see Fig. 2(a) in the Main text). When cellular populations reduce their sensitivity in dose-dependent manner, neither the LQ nor the Jung's model can describe the survival and then, the regression rate of the Umodel (with two extra parameters) is required to describe the cellular population response, providing insight into the recovery mechanisms. Such curves were found for six cell types (Xrs5, HepG2, HUH7, PLC, SW153 and HDF) reported in reference⁶⁶. These results are displayed in Fig. 4 of the main text, and the coefficients and R^2 s are reported in Table 2.

5 Hyperthermia treatment results

We present the optimization results for cell cultures treated with HT, administered via conventional heating techniques such as different types of thermal baths or ovens. The Umodel parameters (r, c, q_{max} and k) are shown in Table 3 (for the HNSCC cell lines from experiments performed in our laboratory), and Tables 4 and 5 (for different cell models found in the literature, treated with HT) with the respective goodness of the fit R^2 of Jung's model for comparison. The survival curves are shown in Figure 1 for our experiments, and in Figures 3 to 5 for literature sources. In our experiments (Table 3, Figure 1), only UT-SCC-14 at 45°C presents adaptation to treatment. In the second block of data (Tables 4) some cell types at certain "mild" temperatures display such a flattening of the logarithmic survival curves (some examples shown in Fig. 2). In the third block of data (Table 5) the most of the data display that behaviour, as shown in Figs. 3 to 5 (summarized in Table I of the Main text for details). Again, on average and in most cases, the Umodel performs better or similarly, providing insights into the cellular population recovery. As it can be observed, the Umodel provides a great advantage to describe logarithmic survival curves exhibiting adaptation to the treatment.

The temperature dependence of the sublethal damage rate displays the exponential behaviour $r = e^{b(T-T_g)}$ predicted and explained in reference³³. Here, b is the slope of the temperature-dependent heat capacity function of the cell, and T_g is the average melting point of cellular proteins undergoing denaturation under the effect of heat. The adjusted values for b and T_g are shown in Table 6. The exponential behaviour of r is also set for q_{max} , to describe the upregulation of the repair mechanisms as a consequence of the damaging stimulus (as explained in the Methods section). The results are graphically shown in Figs. 6 for the cell lines of our experiments, and in Figs. 7 and 8, for data sets from the literature.

6 Combined treatment - additional results

The logarithmic survival of combined sequential thermoradiotherapy is presented in Fig. 9 for two cell lines from our experiments (FaDu and SAS), and for two data sets from literature (HCT116²⁶ and CHO⁶⁹). As explained in the main text, the outcome of the combined therapy comes in the Umodel through the sequential application of the two treatments operators (considering the order in which they were applied), and the detriment of the RT repair mechanisms, reflected in lower values of q_{max} and c . The altered values of r and c are displayed in Tables 8 and 7 for the two data sets of our own (Cell lines SAS and FaDu), and in Tables 9 and 10 for the two data sets from the literature (Cell models HCT116 and CHO). The normalized values of $r_{RT_{new}}$ and $c_{RT_{new}}$ are shown in the main text for SAS and FaDu (Fig. 5), and displayed here in Fig. 10 for HCT116 and CHO.

Table 1. Best fitting parameters of the LQ, Jung's and Umodel to clonogenic survival data from eight HNSCC cell lines exposed to RT.

Cell line	LQ-model			Jungs model			Unified model				
	α [Gy ⁻¹]	β [Gy ⁻²]	R^2	r [Gy ⁻¹]	c [Gy ⁻¹]	R^2	r [Gy ⁻¹]	c [Gy ⁻¹]	q_{max} [Gy ⁻¹]	k [Gy]	R^2
Cal33	0.2223	0.01948	0.994	0.5726	0.3782	0.997	0.6711	0.3781	0.09845	1.274E-04	0.997
HSC4	0.2077	0.02922	0.997	0.8000	0.2530	0.998	5.076	0.06005	4.180	1.242	0.998
SAS	0.2223	0.01832	0.999	0.4885	0.5433	0.999	40.25	0.01582	39.65	0.3553	1.000
FaDu	0.3499	0.01209	0.996	0.5167	1.026	0.999	36.24	0.01473	40.26	1.168	0.999
XF354	0.5423	2.161E-03	0.996	0.5933	2.415	0.997	1.267	0.8052	0.8680	1.242	0.998
UT-SCC-5	0.1802	0.02729	0.997	0.7439	0.2392	0.999	0.7439	0.2392	3.006E-08	1.185	0.999
UT-SCC-14	0.3640	0.05003	1.000	0.9989	0.5036	0.996	40.26	0.07197	38.69	0.06992	0.999
UT-SCC-60A	0.3389	0.05827	0.998	1.142	0.3971	0.992	40.26	0.06563	38.24	0.07037	0.996
UT-SCC-8	0.2753	0.04568	0.999	0.8758	0.4384	0.999	40.26	0.02634	37.97	0.2538	1.000
Average R^2			0.997			0.997					0.999

Table 2. Best fitting parameters of the LQ, Jung's and Umodel to clonogenic survival data from cells exposed to RT, extracted from literature

Cell line	LQ-model			Jungs model			Unified model				
	$\alpha[\text{Gy}^{-1}]$	$\beta[\text{Gy}^{-2}]$	R^2	$r[\text{Gy}^{-1}]$	$c[\text{Gy}^{-1}]$	R^2	$r[\text{Gy}^{-1}]$	$c[\text{Gy}^{-1}]$	$q_{\max}[\text{Gy}^{-1}]$	$k[\text{Gy}]$	R^2
PLC 12C ⁶⁶	1.564	-0.08278	0.992	1.390	16.91	0.983	49.49	64.41	48.31	1.070E-03	0.998
HepG2 ^{12C} ⁶⁶	1.732	-0.1676	0.861	1.338	16.91	0.823	49.08	64.41	48.31	4.003E-03	0.943
HepG2 ^{16O} ⁶⁶	1.312	-0.08920	0.997	1.116	16.91	0.985	23.45	64.41	22.49	1.890E-03	0.998
XRSS ⁶⁸	3.273	-0.5834	0.977	2.759	16.91	0.953	5.061	5.938	48.29	13.60	0.982
HUH7 ⁶⁶	1.900	-0.1287	0.936	1.613	16.91	0.912	49.48	64.41	48.31	2.824E-03	0.972
SW1353 ⁶⁷	1.418	-0.06179	0.999	1.181	16.91	0.987	1.862	64.41	1.066	0.7274	1.000
HDF ⁶⁷	1.241	-0.01334	0.996	1.207	16.91	0.996	1.943	1.730	25.76	99.36	1.000
Average R^2			0.950			0.930					0.980

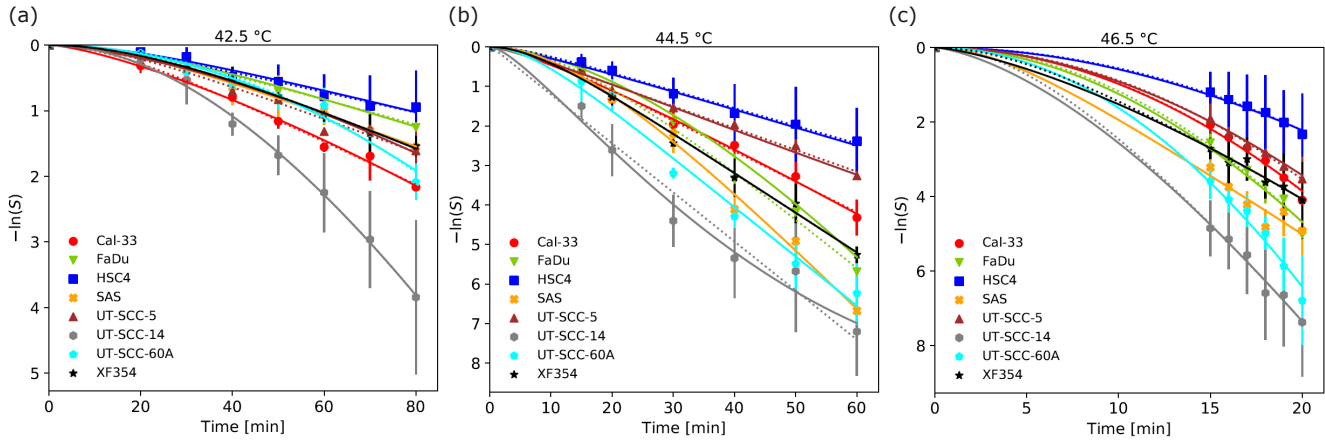


Figure 1. Comparison of LQ and Umodel in HT clonogenic survival experiments in HNSCC cell lines Symbols represent cell survival fractions ($-\ln(S)$) obtained from clonogenic assays using eight human HNSCC cell lines exposed to HT at 42.5°C, 44.5°C and 46.5°C. Continuous lines display the theoretical prediction of the Umodel model, dotted lines prediction of Jung's model.

Table 3. Best fitting parameters of Jung's and Umodel to clonogenic survival data from eight HNSCC cell lines exposed to HT.

T[°C]	Cell line	Jungs model			Unified model				
		$r[\text{min}^{-1}]$	$c[\text{min}^{-1}]$	R^2	$r[\text{min}^{-1}]$	$c[\text{min}^{-1}]$	$q_{\max}[\text{min}^{-1}]$	$k[\text{min}]$	R^2
42.5	HSC4	0.01566	0.06957	0.969	3.287	0.04943	3.270	1.000E-12	0.964
	UT-SCC-5	0.02554	0.06132	0.974	4.479	5.500E-03	4.408	0.1000	0.957
	Cal33	0.03318	0.06229	0.994	3.095	3.146E-03	3.030	0.9999	0.994
	XF354	0.02990	0.03438	0.997	1.599	0.03440	1.569	2.404E-06	0.997
	FaDu	0.01946	0.05566	0.986	0.03147	0.04013	9.290E-03	1.000E-12	0.984
	SAS	0.02558	0.05024	0.996	1.590	0.05022	1.564	1.000E-12	0.996
	UT-SCC-60A	44.06	1.374E-05	0.967	4.715	2.051E-03	4.419	0.02622	0.967
	UT-SCC-14	0.1461	0.01062	0.997	4.275	0.01069	4.130	1.457E-06	0.997
	Average R^2			0.985					0.982
44.5	HSC4	0.04466	0.1897	0.992	10.12	0.05224	10.08	0.01415	0.989
	UT-SCC-5	0.05512	0.3703	0.992	11.68	0.06923	11.63	0.01260	0.990
	Cal33	0.07727	0.1709	0.990	7.705	0.01201	7.641	0.2619	0.990
	XF354	0.1008	0.1198	0.990	5.359	0.1198	5.258	1.000E-12	0.990
	FaDu	0.1267	0.06174	0.994	0.8644	0.01629	0.6649	1.000	0.972
	SAS	0.1548	0.05639	0.992	3.960	0.05639	3.805	3.496E-10	0.992
	UT-SCC-60A	0.1248	0.1334	0.984	13.32	0.1334	13.19	2.946E-09	0.984
	UT-SCC-14	0.1242	3.000	0.972	11.02	9.847E-03	11.31	0.9868	0.983
	Average R^2			0.988					0.986
46.5	HSC4	50.00	2.226E-04	0.995	25.88	0.01601	25.11	1.000E-12	0.991
	UT-SCC-5	16.60	1.073E-03	0.998	35.59	0.01945	34.59	1.000E-12	0.995
	Cal33	50.00	3.872E-04	0.991	21.13	4.946E-03	17.10	3.607E-06	0.990
	XF354	0.2926	0.1566	0.992	16.97	0.02726	16.54	0.1038	0.992
	FaDu	50.00	4.704E-04	0.989	39.39	0.02037	38.08	1.000E-12	0.985
	SAS	0.3185	0.2315	0.979	9.711	0.2299	9.392	7.312E-08	0.979
	UT-SCC-60A	50.00	6.460E-04	0.991	43.95	3.290E-03	33.97	1.000E-12	0.990
	UT-SCC-14	0.5962	0.1178	0.995	28.90	0.04634	28.14	0.03216	0.995
	Average R^2			0.991					0.990

Table 4. Best fitting parameters of Jung’s and Umodel to clonogenic survival data from cells exposed to HT, extracted from literature (sorted by temperature).

T[°C]	Cell line	Jungs model			Unified model				
		r[min^{-1}]	c[min^{-1}]	R^2	r[min^{-1}]	c[min^{-1}]	q_{max} [min^{-1}]	k[min]	R^2
40	CHO ²⁹	4.739E-04	3.000	0.957	1.021	0.01687	1.021	0.01069	0.999
41	CHO ²⁹	6.926E-04	0.1372	0.992	1.415	1.272E-03	1.415	0.1059	0.992
	HeLa ⁶³	9.449E-04	3.000	0.724	2.436E-03	0.9992	1.516E-03	1.000	0.738
	Average R^2	0.858			0.865				
41.5	CHO ²⁹	0.01417	3.476E-03	0.998	1.681	1.156E-03	1.646	0.02991	0.998
41.8	CFU-GM ⁶⁴	6.956E-03	0.02459	0.952	0.2453	0.03850	0.2390	0.01161	0.948
42	CHO ²⁹	0.01754	0.01251	0.985	1.987	1.463E-03	1.931	0.5000	0.990
	HeLa ⁶³	4.187E-03	3.000	0.965	0.01258	1.000	8.589E-03	1.000	0.967
	CFU-GM ⁶⁴	0.01026	3.000	0.984	0.2641	0.03397	0.2574	0.7651	0.994
	Average R^2	0.978			0.984				
42.3	CFU-GM ⁶⁴	0.02013	0.1517	0.980	1.164	0.01039	1.159	0.8850	0.987
42.5	CHO ²⁹	0.03080	0.03389	0.993	2.336	3.340E-03	2.274	0.7424	0.996
	CFU-GM ⁶⁴	0.05723	0.03731	0.998	1.189	0.01842	1.131	0.2963	0.998
	CHO ⁶⁹	46.97	1.825E-06	0.977	0.07062	1.237E-03	5.551E-15	1.240E-11	0.978
	Average R^2	0.989			0.991				
43	CHO ²⁹	0.1129	0.01332	0.997	2.822	3.688E-03	2.585	0.5000	0.996
	HeLa ⁶³	0.01508	3.000	0.992	0.06383	0.1206	0.04937	1.000	0.993
	CFU-GM ⁶⁴	0.1227	0.02698	0.997	11.96	2.254E-03	11.14	0.1193	0.994
	CHO ⁶⁹	0.08833	0.01126	0.995	0.1706	5.122E-03	5.000E-10	7.780E-11	0.994
	Average R^2	0.995			0.994				
43.5	CHO ²⁹	0.1431	0.03210	0.996	3.266	0.03202	3.122	1.000E-12	0.996
44	CHO ²⁹	0.2098	0.02872	0.998	3.988	7.932E-03	3.540	0.3345	0.998
	HeLa ⁶³	0.04043	0.1062	0.985	0.3181	0.03664	0.2810	1.000	0.984
	CFU-GM ⁶⁴	0.2369	0.1233	0.978	50.00	5.735E-03	49.11	0.1426	0.974
	Average R^2	0.987			0.985				
44.5	CHO ²⁹	0.2307	0.08873	0.996	4.684	0.01126	4.162	1.000	0.995
45	CHO ²⁹	0.5219	0.04518	0.998	5.468	0.04501	4.944	2.295E-10	0.998
	HeLa ⁶³	0.08890	0.2156	0.999	1.668	0.02452	1.606	1.000	0.998
	HCT116 ²⁶	0.1915	0.2361	0.986	0.5522	0.2367	0.3608	6.062E-06	0.986
	Cal27 ²⁶	0.2341	0.01455	0.996	0.8259	0.01464	0.5928	5.705E-09	0.996
	Average R^2	0.995			0.994				
46	HCT116 ²⁶	0.3569	0.5707	0.992	1.875	0.1448	1.636	1.000	0.993
	Cal27 ²⁶	0.3798	0.03764	0.995	1.860	0.03751	1.480	3.292E-12	0.995
	Average R^2	0.994			0.994				
47	HCT116 ²⁶	0.6864	0.9470	0.987	6.790	0.1679	6.390	0.3762	0.988
	Cal27 ²⁶	0.6350	0.2128	0.991	4.250	0.2128	3.615	1.000E-12	0.991
	Average R^2	0.989			0.990				
48	HCT116 ²⁶	1.989	0.6598	0.997	28.39	0.6601	26.40	2.196E-11	0.997
	Cal27 ²⁶	1.144	0.5583	0.992	9.986	0.2982	8.858	0.05522	0.992
	Average R^2	0.994			0.995				

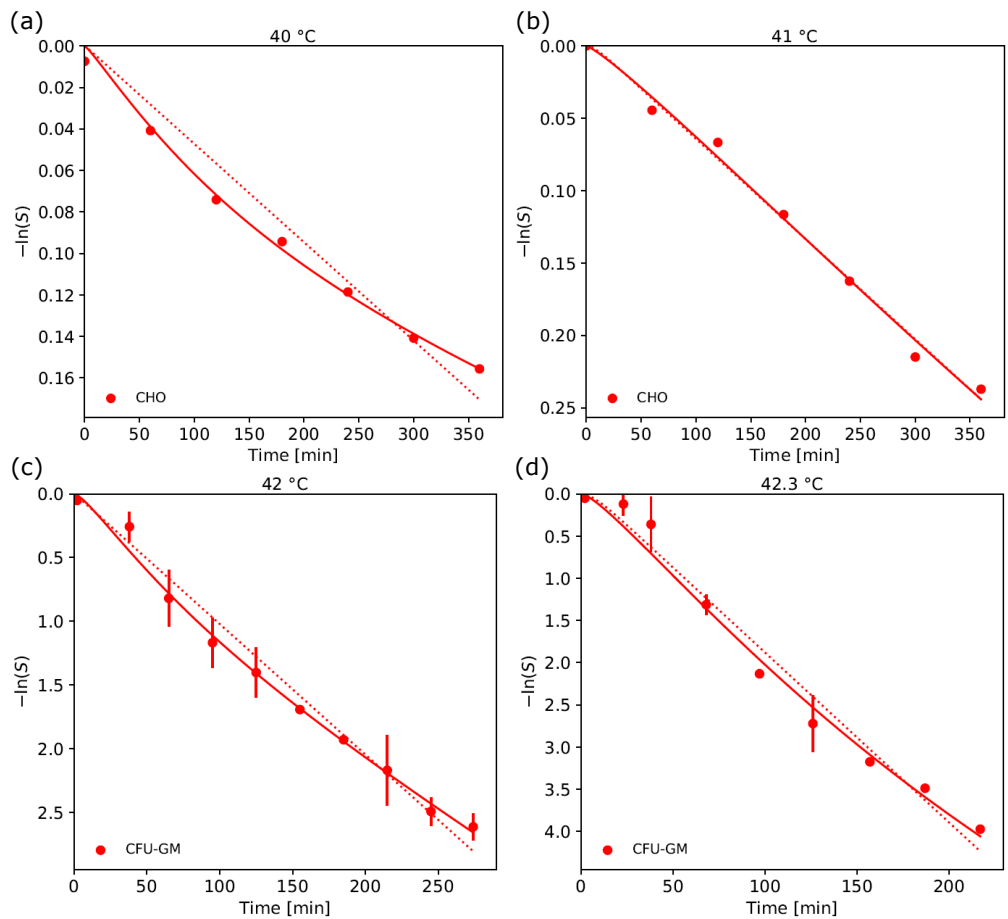


Figure 2. Comparison of Jung's and Umodel in HT clonogenic survival experiments displaying adaptation to treatment - example 1. Symbols represent cell survival fractions ($-\ln(S)$) obtained from clonogenic assays from CHO cells are shown in panels (a,b)²⁹ and CFU-GM cells in panels (c,d)⁶⁴. Continuous lines display the theoretical prediction of the Umodel, dotted lines prediction of Jung's model.

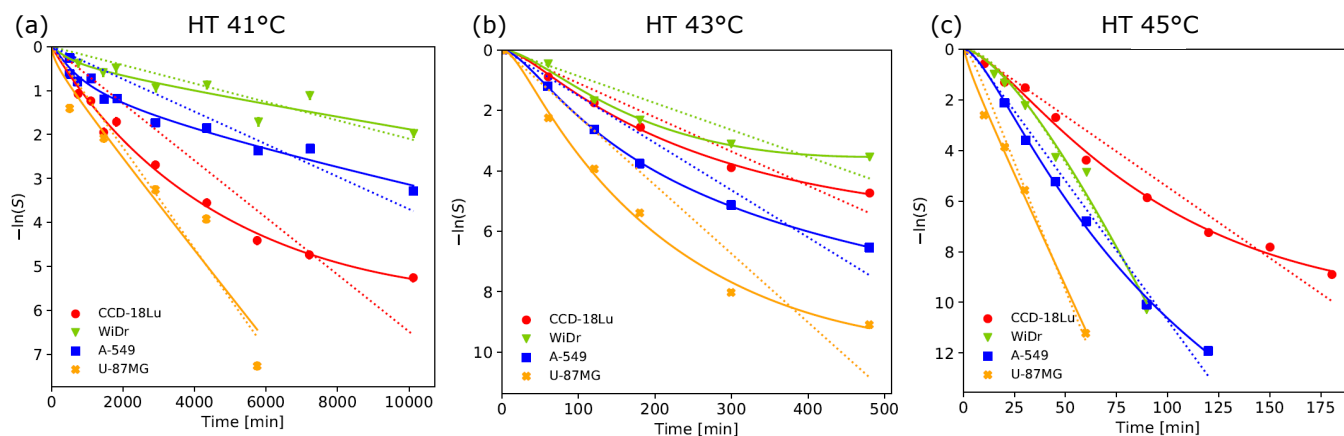


Figure 3. Comparison of fittings of Jung's and Umodel in HT clonogenic survival experiments displaying adaptation to treatment - example 2. Symbols represent cell survival fractions ($-\ln(S)$) obtained from HT clonogenic assays at 41 °, 43 °C and 45 ° extracted from⁶⁵. Continuous lines display the theoretical prediction of the Umodel, dotted lines prediction of Jung's model

Table 5. Best fitting parameters of Jung's and Umodel to clonogenic survival data from cells exposed to HT, extracted from the literature; upper panel from⁶⁵, middle and lower panels from³² and⁴⁷, respectively.

T[°C]	Cell line	Jungs model			Unified model				
		r[min^{-1}]	c[min^{-1}]	R^2	r[min^{-1}]	c[min^{-1}]	q_{max} [min^{-1}]	k[min]	R^2
41	CCD-18Lu	6.488E-04	0.3500	0.846	1.360E-03	1.667	1.811E-03	4.800E+03	0.993
	WiDr	2.098E-04	0.3500	0.827	4.758E-03	6.731E-03	4.628E-03	21.41	0.898
	A-549	3.701E-04	0.3500	0.824	9.724E-03	3.790E-03	9.558E-03	27.90	0.978
	U-87MG	1.150E-03	0.3500	0.924	6.981E-03	1.667	5.970E-03	18.25	0.933
	Average R^2	0.855			0.950				
43	CCD-18Lu	0.01131	0.3500	0.939	0.02598	0.03692	0.03287	219.8	0.998
	WiDr	8.906E-03	0.3500	0.872	0.06704	0.01156	0.07521	44.29	0.995
	A-549	0.01562	0.3500	0.928	0.09815	0.01942	0.09821	24.80	1.000
	U-87MG	0.02270	0.3500	0.885	0.05522	0.06053	0.07186	198.2	0.997
	Average R^2	0.906			0.998				
45	CCD-18Lu	0.05604	0.3500	0.961	0.5259	0.02181	0.5498	9.812	0.995
	WiDr	0.1433	0.04858	0.982	1.157	0.01426	1.000	2.466	0.985
	A-549	0.1103	0.3500	0.984	1.006	0.03142	1.000	4.760	0.999
	U-87MG	0.2018	0.3500	0.979	0.7644	1.667	0.5922	0.2782	0.996
	Average R^2	0.976			0.994				
41.5	CHO ³²	7.241E-04	6.300	0.684	0.02198	4.595E-03	0.02286	13.31	0.801
42	CHO ³²	1.774E-03	6.300	0.659	0.05258	0.01353	0.05327	6.349	0.973
42.5	CHO ³²	0.01110	6.300	0.884	0.09794	4.640E-03	0.1308	133.8	0.987
43	CHO ³²	15.00	4.241E-05	0.961	0.4595	1.609E-03	0.2191	266.0	0.950
43.5	CHO ³²	15.00	1.097E-04	0.965	1.221	2.450E-03	0.5040	4.385E-05	0.960
44	CHO ³²	15.00	3.838E-04	0.921	2.504	4.704E-03	1.219	3.348E-12	0.916
45.5	CHO ³²	15.00	1.664E-03	0.978	25.59	3.289E-03	17.92	3.348E-12	0.978
42.2	CHO ⁴⁷	9.180E-03	21.00	0.886	0.08300	5.457E-03	0.1048	80.00	0.995
42.3	CHO ⁴⁷	9.822E-03	21.00	0.861	0.09401	7.441E-03	0.1082	47.80	0.988
42.4	CHO ⁴⁷	0.01204	21.00	0.922	0.1043	8.016E-03	0.1161	43.16	0.991
42.5	CHO ⁴⁷	0.01687	21.00	0.804	0.1104	9.998E-03	0.1349	79.99	0.991

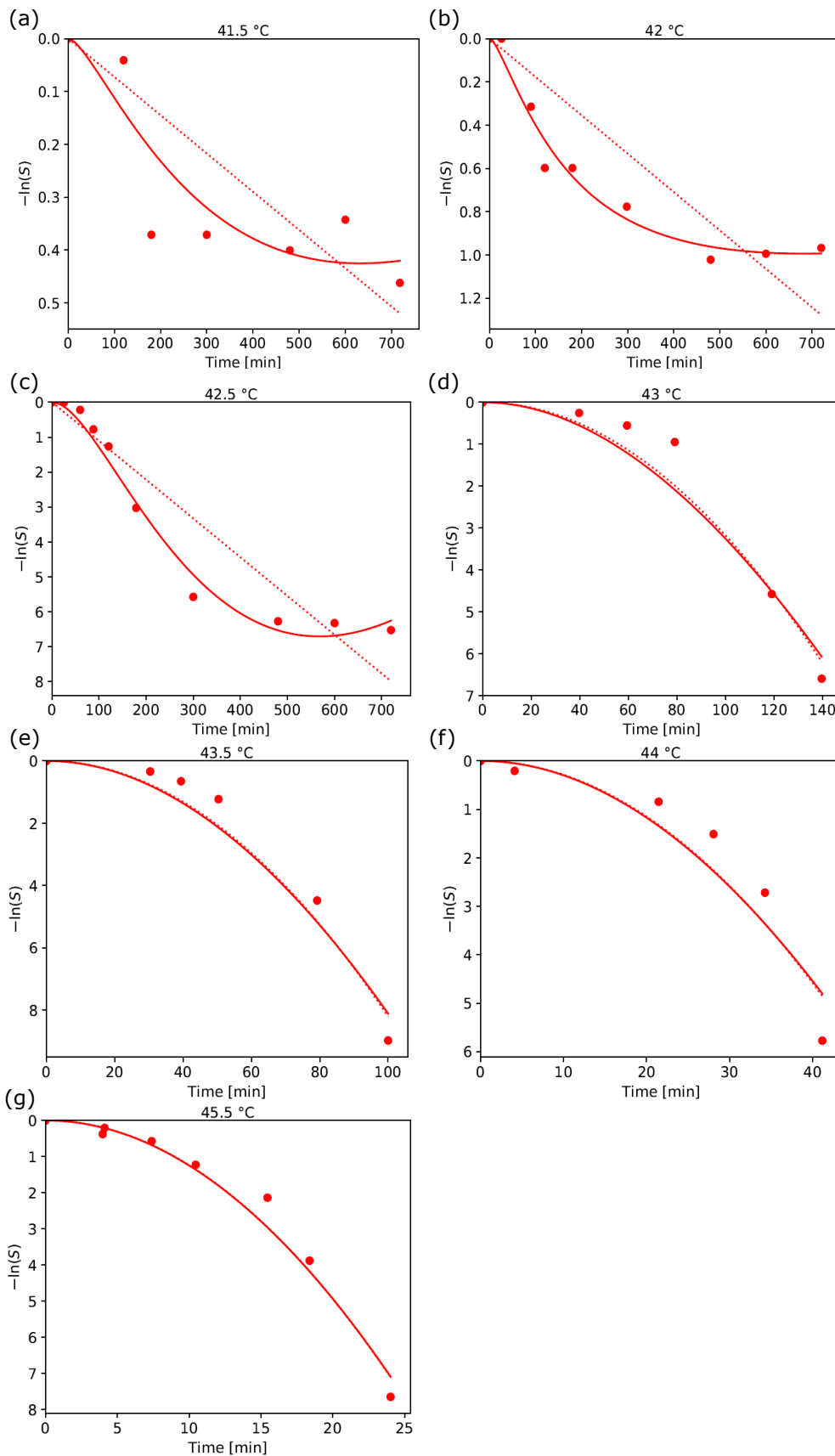


Figure 4. Comparison of fittings of Jung's and Umodel in HT clonogenic survival experiments displaying adaptation to treatment - example 3³². Symbols represent cell survival fractions ($-\ln(S)$) obtained from clonogenic assays. Continuous lines display the theoretical prediction of the Umodel, dotted lines prediction of Jung's model. Lower temperatures display adaptation to treatment.

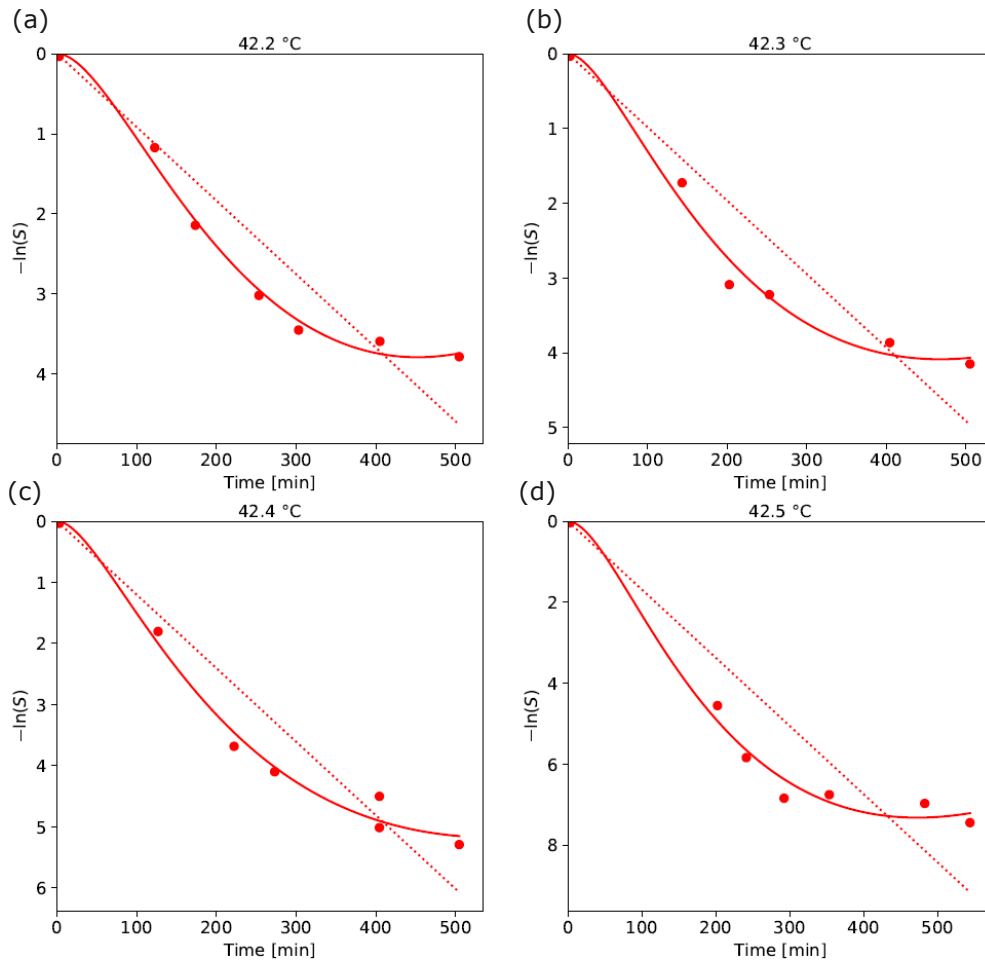


Figure 5. Comparison of fittings of Jung's and Umodel in HT clonogenic survival experiments displaying adaptation to treatment - example 447. Symbols represent cell survival fractions ($-\ln(S)$) obtained from clonogenic assays. Continuous lines display the theoretical prediction of the Umodel, dotted lines prediction of Jung's model. All temperatures display adaptation to treatment.

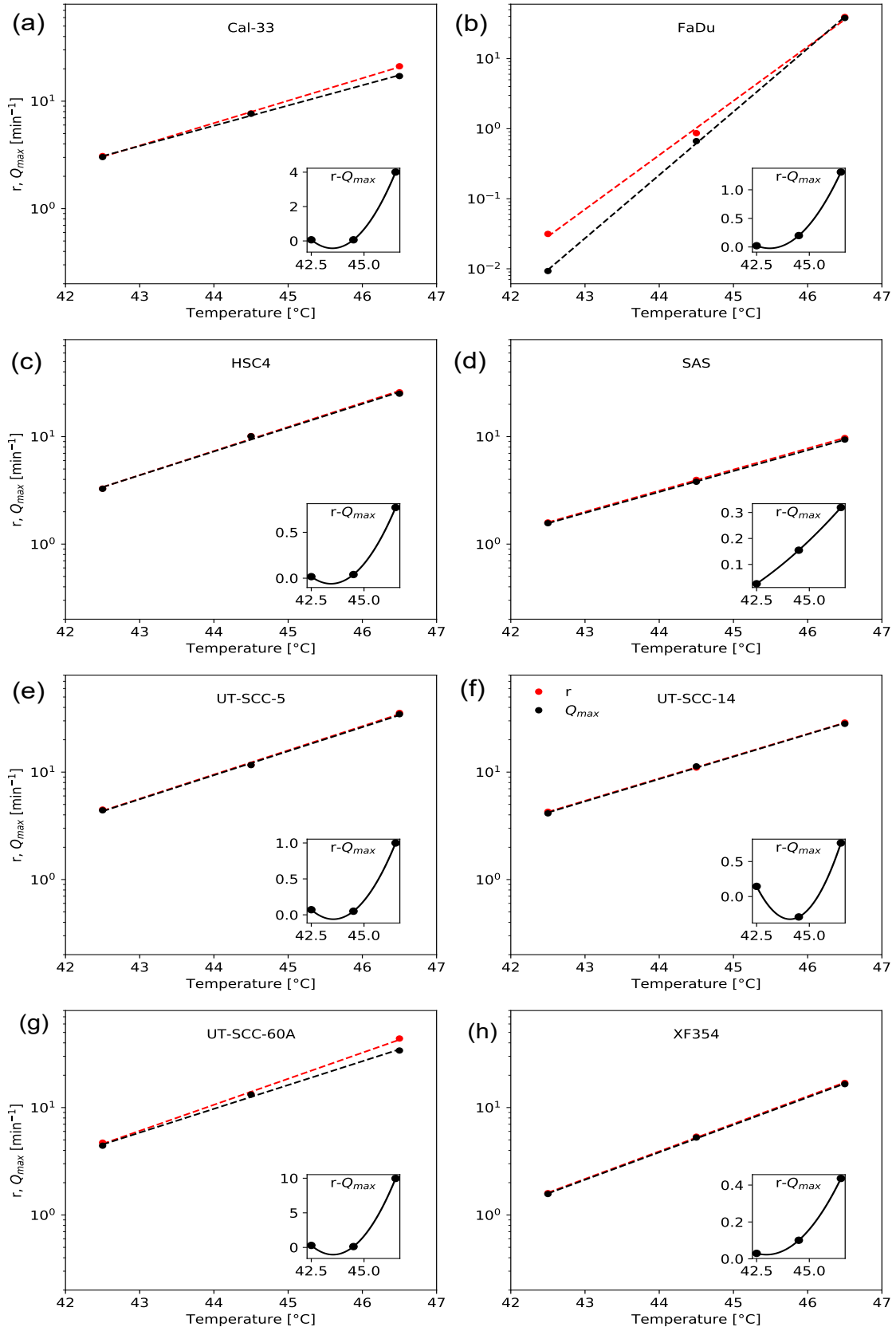


Figure 6. Advance rate in the SLD chain r , and maximum repair rate q_{max} as functions of the HT temperature for the clonogenic survival curves from eight HNSCC cell lines exposed to HT. In the insets the difference between the two parameters in linear scale.

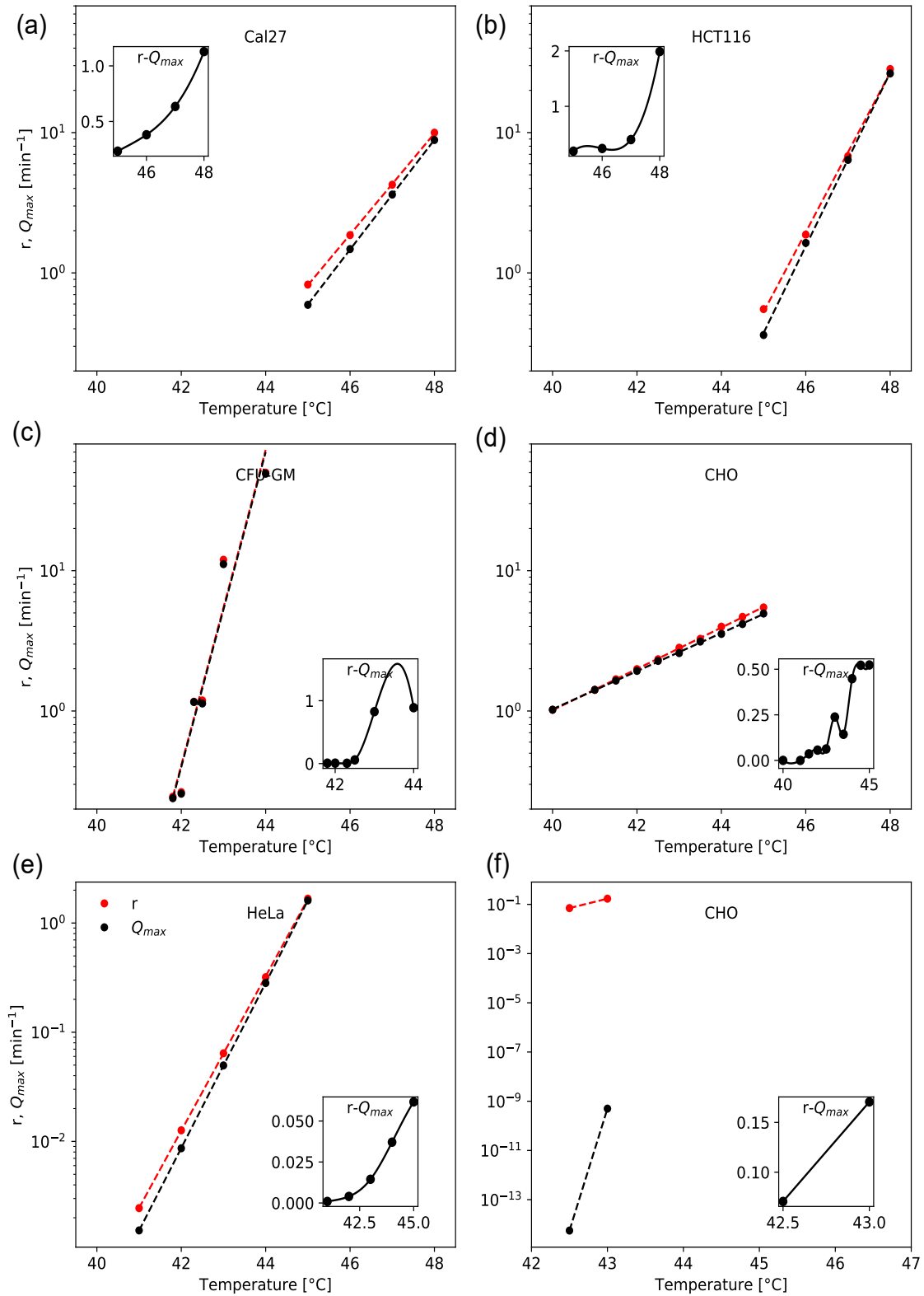


Figure 7. Advance rate in the SLD chain r , and maximum repair rate q_{max} as functions of the HT temperature for the clonogenic survival curves from cells exposed to HT, extracted from literature. In the insets the difference between the two parameters in linear scale. (a) HeLa⁶³, (b) CFU-GM⁶⁴, (c) HCT116²⁶, (d) Cal27²⁶, (e) CHO²⁹, (f) CHO⁶⁹.

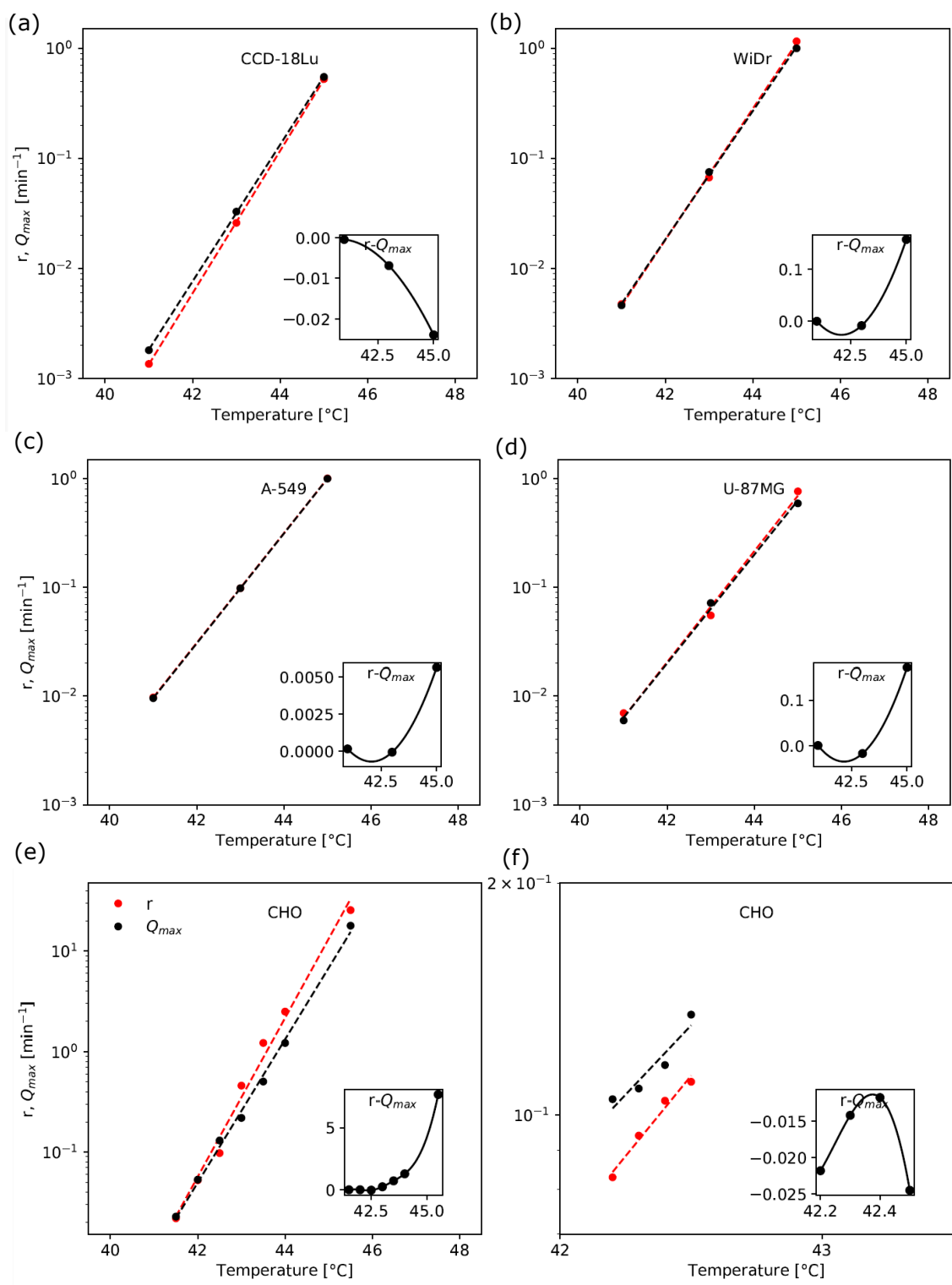


Figure 8. Advance rate in the SLD chain r , and maximum repair rate q_{max} as functions of the HT temperature for the clonogenic survival curves from cells exposed to HT, extracted from literature. In the insets the difference between the two parameters in linear scale. (a-d) ⁶⁵, (e) CHO³², (f) CHO⁴⁷.

Table 6. Exponential behaviour of the sublethal damage accumulation rate. Parameters and coefficient of determination for all the cell models of this study. Below the line results for data sets extracted from literature are listed.

Cell line	b [min ⁻¹]	Tg [min]	R ²
SAS	0.452	41.5	1.000
FaDu	1.783	44.5	0.998
Cal33	0.480	40.2	0.999
HSC4	0.516	40.1	0.997
XF354	0.591	41.7	1.000
UT-SCC-5	0.518	39.7	0.998
UT-SCC-14	0.478	39.5	1.000
UT-SCC-60A	0.558	39.8	0.998
HeLa	1.629	44.7	1.000
CFU-GM	2.587	42.3	0.953
HCT116	1.311	45.5	0.999
Cal27	0.830	45.2	1.000
CHO ²⁹	0.339	40.0	1.000
CHO ⁶⁹	1.764	44.0	1.000
18Lu ⁶⁵	1.489	42.7	1.000
WiDr ⁶⁵	1.373	41.9	1.000
A549 ⁶⁵	1.160	41.5	1.000
U87MG ⁶⁵	1.173	41.8	0.995
CHO ³²	1.822	42.9	0.988
CHO ⁴⁷	0.960	44.8	0.975

Table 7. Umodel fitting parameters to clonogenic survival data from FaDu cell line exposed to TRT. In all cases $q_{\max} = 0.4555 \text{ Gy}^{-1}$ and $k = 0.596 \text{ Gy}$.

T[°C]	HT time [min]	$r_{\text{new}}[\text{Gy}^{-1}]$	$c_{\text{new}}[\text{Gy}^{-1}]$	TER = $\frac{r_{\text{new}}}{r_{\text{old}}}$	R ²
40.5	0.0	1.610	0.327	1.000	0.992
	15.0	2.703	0.115	1.679	0.970
	17.5	2.886	0.118	1.792	0.993
	20.0	3.067	0.104	1.905	0.975
	30.0	3.791	0.073	2.354	0.946
42.5	0.0	1.610	0.327	1.000	0.992
	15.0	3.541	0.085	2.199	0.964
	17.5	3.888	0.093	2.414	0.992
	20.0	4.189	0.076	2.602	0.950
	30.0	5.487	0.059	3.408	0.948
44.5	0.0	1.610	0.327	1.000	0.949
	15.0	4.194	0.057	2.605	0.981
	17.5	4.624	0.064	2.871	0.990
	20.0	5.064	0.059	3.145	0.962

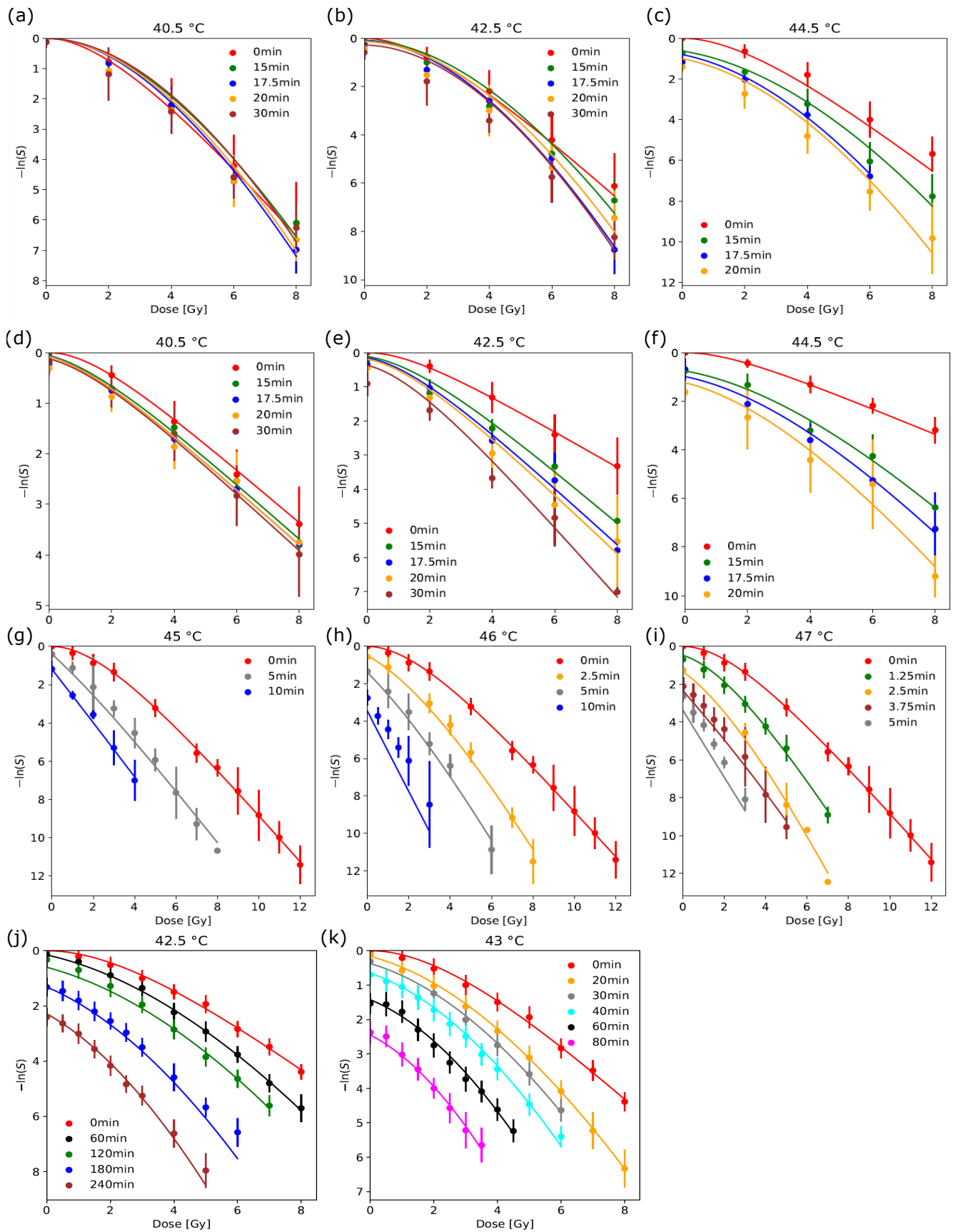


Figure 9. Umodel fittings for the combined thermoradiotherapy. Symbols represent cell survival fractions ($-\ln(S)$) obtained from clonogenic assays from FaDu(a,b,c) and SAS (d,e,f) HNSCC cell lines, HCT116 cells²⁶ (g,h,i), and CHO cell line⁶⁹ (j,k), exposed to combined TRT with interval between the treatments effectively null. Continuous lines display the theoretical prediction of the Umodel.

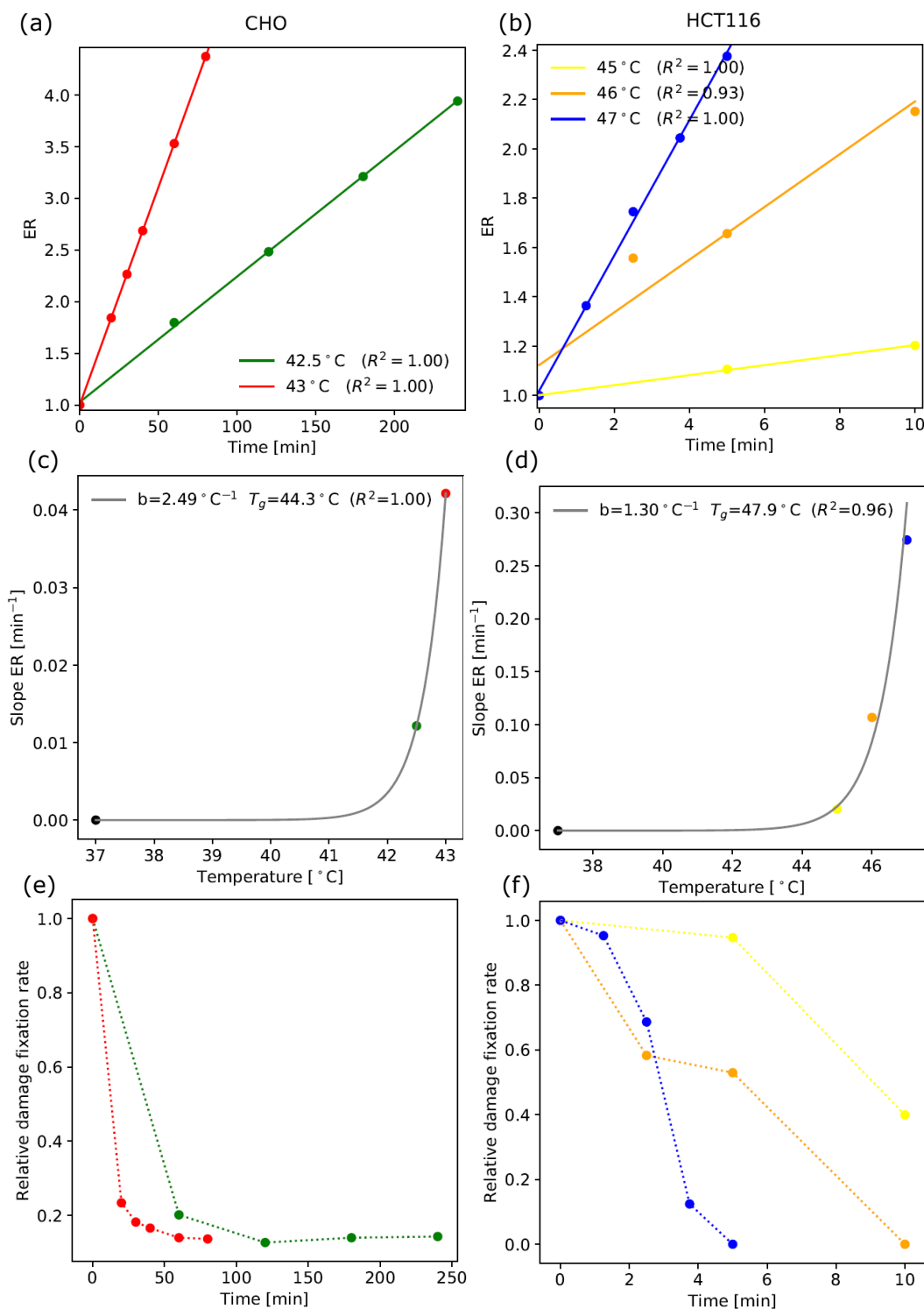


Figure 10. Enhancement of radiation by HT as a function of exposure time and temperature. (a,b) linear dependency of the enhancement ratios ER with HT treatment time. (c,d) slopes from (a) and (b) respectively, as function of HT temperature. (e,f) relative damage fixation rate C_{RTnew}/C_{RTold} as function of HT treatment time.

Table 8. Umodel fitting parameters to clonogenic survival data from SAS cell line exposed to TRT. In all cases $q_{\max} = 2.465E-07 \text{ Gy}^{-1}$ and $k = 1.242 \text{ Gy}$.

T[°C]	HT time [min]	$r_{\text{new}}[\text{Gy}^{-1}]$	$c_{\text{new}}[\text{Gy}^{-1}]$	TER = $\frac{r_{\text{new}}}{r_{\text{old}}}$	R^2
40.5	0.0	0.525	0.623	1.000	0.999
	15.0	0.547	0.515	1.040	0.996
	17.5	0.548	0.569	1.043	0.997
	20.0	0.549	0.560	1.045	0.981
	30.0	0.568	0.540	1.081	0.997
42.5	0.0	0.525	0.623	1.000	0.999
	15.0	0.778	0.476	1.482	0.986
	17.5	0.835	0.552	1.591	0.992
	20.0	0.867	0.552	1.650	0.972
	30.0	1.030	0.552	1.961	0.971
44.5	0.0	0.525	0.623	1.000	0.992
	15.0	1.405	0.144	2.676	0.988
	17.5	1.551	0.152	2.953	0.991
	20.0	1.701	0.171	3.239	0.962

Table 9. Umodel fitting parameters to clonogenic survival data from HCT116 cell line exposed to TRT²⁶. In all cases $q_{\max} = 0.1280 \text{ Gy}^{-1}$ and $k = 0.1161 \text{ Gy}$.

T[°C]	HT time [min]	$r_{\text{new}}[\text{Gy}^{-1}]$	$c_{\text{new}}[\text{Gy}^{-1}]$	TER = $\frac{r_{\text{new}}}{r_{\text{old}}}$	R^2
45	0.0	1.359	0.338	1.000	0.999
	5.0	1.504	0.320	1.107	0.989
	10.0	1.635	0.135	1.203	0.990
46	0.0	1.359	0.338	1.000	0.999
	2.5	2.116	0.197	1.557	0.991
	5.0	2.251	0.179	1.656	0.986
	10.0	2.924	0.000	2.151	0.554
47	0.0	1.359	0.338	1.000	0.999
	1.25	1.854	0.322	1.364	0.995
	2.5	2.372	0.232	1.745	0.993
	3.75	2.778	0.042	2.044	0.973
	5.0	3.228	0.000	2.375	0.797

Table 10. Umodel fitting parameters to clonogenic survival data from CHO cell line exposed to TRT⁶⁹. In all cases $q_{\max} = 1.059 \text{ Gy}^{-1}$ and $k = 2.187E-10 \text{ Gy}$.

T[°C]	HT time [min]	$r_{\text{new}}[\text{Gy}^{-1}]$	$c_{\text{new}}[\text{Gy}^{-1}]$	TER = $\frac{r_{\text{new}}}{r_{\text{old}}}$	R^2
42.5	0.0	1.918	0.308	1.000	0.996
	60.0	3.446	0.062	1.797	0.999
	120.0	4.761	0.039	2.483	0.991
	180.0	6.157	0.043	3.210	0.964
	240.0	7.557	0.044	3.940	0.988
43	0.0	1.918	0.308	1.000	0.996
	20.0	3.534	0.072	1.843	0.999
	30.0	4.343	0.056	2.264	0.998
	40.0	5.151	0.051	2.686	0.994
	60.0	6.768	0.043	3.529	0.991
	80.0	8.385	0.042	4.372	0.991